Modelling high redshift Lyman α emitters

T. Garel,[1]★ J. Blaizot,[1] B. Guiderdoni,[1] D. Schaerer,[2,3] A. Verhamme[1] and M. Hayes[2,3]

[1]*Centre de Recherche Astrophysique de Lyon, Université de Lyon, Université Lyon 1, Observatoire de Lyon, Ecole Normale Supérieure de Lyon, CNRS, UMR 5574, 9 avenue Charles André, Saint Genis Laval F-69230, France*
[2]*Observatoire de Genève, Université de Genève, 51, Ch. des Maillettes, CH-1290 Versoix, Switzerland*
[3]*CNRS, IRAP, 14 Avenue E. Belin, F-31400 Toulouse, France*

ABSTRACT

We present a new model for high redshift Lyman α emitters (LAEs) in the cosmological context which takes into account the resonant scattering of Lyα photons through expanding gas. The GALICS semi-analytic model provides us with the physical properties of a large sample of high redshift galaxies. We implement, in post-processing, a gas outflow model for each galaxy based on simple scaling arguments. The coupling with a library of numerical experiments of Lyα transfer through expanding (or static) dusty shells of gas allows us to derive the Lyα escape fraction and profile of each galaxy. Results obtained with this new approach are compared with simpler models often used in the literature.

The predicted distribution of Lyα photons escape fraction shows that galaxies with a low star formation rate (SFR) have a f_{esc} of the order of unity, suggesting that, for those objects, Lyα may be used to trace the SFR assuming a given conversion law. In galaxies forming stars intensely, the escape fraction spans the whole range from 0 to 1. The model is able to get a good match to the ultraviolet (UV) and Lyα luminosity function data at $3 < z < 5$. We find that we are in good agreement with both the bright Lyα data and the faint LAE population observed by Rauch et al. at $z = 3$ whereas a simpler *constant Lyα escape fraction* model fails to do so. Most of the Lyα profiles of our LAEs are redshifted by the diffusion in the expanding gas which suppresses intergalactic medium absorption and scattering. The bulk of the observed Lyα equivalent width (EW) distribution is recovered by our model, but we fail to obtain the very large values sometimes detected. Our predictions for stellar masses and UV luminosity functions of LAEs show a satisfactory agreement with observational estimates. The UV-brightest galaxies are found to show only low Lyα EWs in our model, as it is reported by many observations of high redshift LAEs. We interpret this effect as the joint consequence of old stellar populations hosted by UV-bright galaxies, and high H I column densities that we predict for these objects, which quench preferentially resonant Lyα photons via dust extinction.

Key words: radiative transfer – galaxies: evolution – galaxies: formation – galaxies: high-redshift.

1 INTRODUCTION

High-redshift star-forming galaxies are expected to produce strong Lyα emission lines (Partridge & Peebles 1967; Charlot & Fall 1993; Valls-Gabaud 1993). Massive, hot stars are intense sources of hydrogen-ionizing UV photons which turn part of the interstellar medium (ISM) gas into H II regions. Lyα photons are produced by recombination of this gas. Although high-redshift Lyα emitting galaxies have long been sought without success, the number of detections has grown quickly during the last decade, thanks to narrow-band searches (Hu, Cowie & McMahon 1998; Ouchi et al.

2003; Shimasaku et al. 2006; Ouchi et al. 2008; Hu et al. 2010; Ouchi et al. 2010), deep spectroscopic follow-ups of ultraviolet (UV)-selected galaxies (Shapley et al. 2003; Tapken et al. 2007), and deep spectroscopic blind searches (Van Breukelen, Jarvis & Venemans 2005; Rauch et al. 2008).

Although observed samples of high redshift Lyman α emitters (LAEs) have become large enough to derive statistical constraints [e.g. Lyα and UV luminosity functions (LF)], uncertainties remain as a result of measurement errors and differences in survey detection thresholds. The physics involved in LAEs, and especially their Lyα escape fractions, are still poorly understood. Indeed, the travel of Lyα photons from their emission regions through the galaxy and the intergalactic medium (IGM) is complicated. The resonant nature of the Lyα line increases dramatically the travelling path of the photons

★E-mail: tgarel@astro.swin.edu.au

Table 1. Non-exhaustive summary of existing Lyα cosmological models in the literature. SAM: semi-analytic model; PS: Press–Schechter formalism; ST: Sheth–Tormen formalism; PMM: particle multi mesh; RT: radiation transfer

Article	Model	Lyα model	Lyα LF	UV LFs of LAEs	UV LFs	IGM	σ_8
Le Delliou et al. (2006)	SAM (GALFORM)	f_{esc} = const.	Yes	No	No	no	0.93
Mao et al. (2007)	ST	$f_{esc} = f_{IGM} \times e^{-A_\lambda/1.08}$	Yes	No	Yes	yes	0.80
Kobayashi, Totani & Nagashima (2007, 2010)	SAM (Mitaka)	f_{esc} = const./screen/slab	Yes	Yes	Yes	yes	0.90
Nagamine et al. (2010)	GADGET2	f_{esc} = const./Duty cycle	Yes	Yes	Yes	yes	0.90
Tilvi et al. (2009)	GADGET2	f_{esc} = 1/Duty cycle	Yes	No	No	no	0.82
Samui, Srianand & Subramanian (2009)	PS–ST	f_{esc} = const./Duty cycle	Yes	Yes	Yes	no	0.80
Zheng et al. (2010)	PMM N body	RT in IGM (no dust)	Yes	Yes	Yes	yes	0.82
Dayal, Ferrara & Gallerani (2008)	GADGET2	$f_{esc} = \exp(-\tau_{IGM}) \times$ const.	Yes	Yes	No	yes	0.82
This paper	SAM (GALICS)	f_{esc} = RT	Yes	Yes	Yes	Yes	0.76

in the optically thick interstellar gas, enhancing dust absorption even in metal-poor galaxies. Spectroscopic studies of Lyα emitting galaxies (Kunth et al. 1998; Pettini et al. 2001; Dawson et al. 2002; Shapley et al. 2003; Tapken et al. 2004, 2006, 2007) have shown that the line profile is complex, and can have many shapes (P-Cygni, redward asymmetry, double bump). The measure of the interstellar absorption lines with respect to Lyα by Shapley et al. (2003) suggests that gas outflows (probably triggered by supernova feedback) of neutral hydrogen take place in those galaxies. Recent spectroscopic measurements led by McLinden et al. (2011) in two $z \sim 3$ LAEs support this idea. An expanding shell of gas surrounding the galaxy is often proposed as an explanation of this feature and the general shape of the Lyα line (Tenorio-Tagle et al. 1999; Mas-Hesse et al. 2003; Verhamme, Schaerer & Maselli 2006; Dijkstra & Loeb 2008).

In the past years, there has been an intense investigation on the properties of LAEs in the context of hierarchical galaxy formation, through semi-analytic or 'hybrid' models, or numerical simulations (e.g. Le Delliou et al. 2005, 2006; Kobayashi et al. 2007; Samui et al. 2009; Nagamine et al. 2010). Although the implementation of galaxy formation processes include state-of-the-art prescriptions, the modelling of the complicated mechanisms of Lyα photons transfer in galaxies, and their escape from the galaxies, is usually very sketchy. The authors frequently assume a *constant Lyα escape fraction* model, and try to reproduce data (i.e. Lyα luminosity functions) by adjusting the escape fraction as a free parameter ($f_{esc} = 0.02 - 0.60$ at $3 < z < 6$ according to models). This approach appears to work in a satisfactory way, as far as it is possible to get a fit of the bright end of the LAE Lyα luminosity function. However, the deduced value of the free parameter f_{esc} is not 'explained', and these models fail to reproduce the faint LAE population reported by Rauch et al. (2008) at $z \sim 3$, down to a flux of $\sim 10^{-18}$ erg s^{-1} cm^{-2}.

A *duty cycle* scenario (in which only a fraction of the galaxies are turned on as LAEs at a given time, or are able to be detected because of selection criteria) has also been invoked to reproduce the observed Lyα LF. Nagamine et al. (2010) report that a stochastic scenario is favoured compared to a *constant Lyα escape fraction* model as a result of the comparison with observational data. For the *duty cycle* model, they require a fraction of star-forming galaxies observable as LAEs at a given time equal to 0.07 (0.20) at $z = 3$ (6). Samui et al. (2009) fit their free parameters which contain the Lyα escape fraction and the number of galaxies turned on as LAEs, on the observed Lyα LFs and UV LFs of LAEs. Their *duty cycle* parameter has to vary with redshift in order to agree with the data.

Tilvi et al. (2009) relate the Lyα luminosity to the halo mass accretion rate, and are able to reproduce the observed Lyα LF by fitting a single parameter, namely the product of the star formation efficiency and the Lyα time-scale. However, they assume that all Lyα photons are able to escape their model galaxies ($f_{esc} = 1$), which is not consistent with observations of LAEs and Lyman break galaxies (LBGs, e.g. Hayes et al. 2010).

More physical models, taking into account the properties of the galaxies (assuming slab and screen-type dust attenuation), have been investigated by Kobayashi et al. (2007, 2010) and Mao et al. (2007). Kobayashi et al. (2007, 2010) need two free parameters to reproduce the Lyα LF data over the redshift range $3 < z < 6$. Mao et al. (2007) reproduce the Lyα LFs data at $z = 4.9, 5.7$ and 6.4, but they need to vary the IGM transmission.

In parallel to these empirical approaches, several Lyα radiation transfer codes have been developed (Zheng & Miralda-Escudé 2002; Dijkstra et al. 2006; Hansen & Oh 2006; Verhamme, Schaerer & Maselli 2006; Laursen & Sommer-Larsen 2007) including different physics such as dust, gas kinematics, geometry, deuterium, etc. Zheng et al. (2010) perform Lyα radiative transfer through the circumgalactic medium in a cosmological box, but they do not incorporate dust into their model and do not resolve galaxies. Laursen, Sommer-Larsen & Andersen (2009) focus on a few high-resolution galaxies, but the CPU cost of such experiments does not allow one to process large samples of objects. Indeed, carrying out Lyα line transfer in large simulated volumes, and with a resolution high enough to describe the ISM structure and kinematics, is out of CPU reach today. Hence, the need for simplified semi-analytic models remains. A non-exhaustive summary of the LAE models in the literature is given in Table 1.

The purpose of this paper is to make one step further towards a more realistic semi-analytic approach. To this aim, we present a new model for Lyα emission from high redshift galaxies, which relies on two main ingredients. First, we use GALICS (for Galaxies in Cosmological Simulations), a hybrid model of hierarchical galaxy formation in which galaxy formation and evolution are described as the post-processing of outputs of numerical simulations of a large cosmological volume of dark matter (DM, Hatton et al. 2003). Second, we use a large library of radiation transfer models (Schaerer et al. 2011) computed with an updated version of MCLYA (Verhamme et al. 2006), which describes the Lyα transfer through spherical expanding or static shells[1] of neutral gas and dust. We implement a simple shell model in post-processing of GALICS, based on scaling arguments, to infer the shell parameters of the MCLYA library for each model galaxy.

---

[1] Note that our model does not include Lyα radiative transfer through infalling gas.

The advantage of this model with respect to *constant Lyα escape fraction* models is that it computes the Lyα escape fraction of each model galaxy according to its physical properties. In addition, it improves on *screen* or *slab* models by including the resonant radiative transfer of the Lyα line, and by assuming a geometry and kinematics suggested by the observations. With this new tool, we are able to compare our results with existing statistical data such as Lyα and UV LFs, Lyα equivalent width (EW) distributions, stellar masses and the Ando effect (see Ando et al. 2006; Kobayashi et al. 2010).

The outline of the paper is as follows. We describe the GALICS galaxy formation model in Section 2, and the Lyα and shell models in Section 3. In Section 4, we present the distributions of Lyα escape fractions we predict, and the Lyα LFs they yield. We discuss how these LFs are impacted by (i) EW selections and (ii) IGM transmission. In Section 5, we show that our model matches most statistical constraints (Lyα EW distributions, UV LFs of LAEs, stellar masses and the Ando effect), and we use it to discuss their origin. Finally, Section 6 summarizes the results and gives a brief discussion.

2 THE GALICS HYBRID MODEL

In this paper, we use an updated version of the GALICS model (Hatton et al. 2003; Blaizot et al. 2004). We briefly describe the relevant details below.

2.1 Dark matter simulation

We use a DM cosmological simulation run by the Horizon project[2] using the public version of GADGET[3] (Springel 2005). This simulation uses 1024^3 particles of mass $m_p \sim 8.5 \times 10^7 \, M_\odot$ to describe the formation and evolution of DM structures in a comoving volume of $100 \, h^{-1}$ Mpc on a side. It assumes a cosmology and initial conditions which are consistent with *Wilkinson Microwave Anisotropy Probe* (*WMAP*) third year results (Spergel et al. 2007), namely, $h = 0.73$, $\Lambda = 0.76$, $\Omega_m = 0.24$, $\Omega_b = 0.04$ and $\sigma_8 = 0.76$.

About 100 snapshots were saved to disc, regularly spaced in expansion factor by $\delta_a = 0.01$. We processed each of these snapshots to identify DM haloes with a friends-of-friends (FOF) algorithm, using a linking length $b = 0.20$ and keeping only groups with more than 20 particles, i.e. more massive than $1.7 \times 10^9 \, M_\odot$. This mass resolution is sufficient for our this study, which adresses galaxy formation after reionization ($z < 5$), when we expect the IGM's temperature to prevent gas from collapsing within DM haloes of lower masses (e.g. Okamoto, Gao & Theuns 2008). Finally, we follow Tweed et al. (2009) to construct merger trees from our halo catalogues at all timesteps.

2.2 Baryonic prescriptions

The version of GALICS we use here is an update from Hatton et al. (2003) and Cattaneo et al. (2008), with three major differences which are relevant for this study: (i) the way galaxies get their gas, (ii) the way galaxies form stars and (iii) the way we compute extinction of UV light by dust.

First, the new paradigm that has emerged in recent years about gas supply into high redshift galaxies (e.g. Dekel & Birnboim 2006) has led us to replace the classical gas cooling mechanism by filamentary accretion of cold gas. In practice, for the redshift range which we explore here ($3 < z < 5$), this means that galaxies accrete gas from

the IGM at a rate directly proportional to the halo growth, with a delay set by the free-fall time instead of the cooling time.

Secondly, we use a Kennicutt-type law to model star formation. The low value of σ_8 from *WMAP* third year results has led us to enhance star formation significantly compared to the local law of Kennicutt (1998), in order to fit high-redshift observations. In practice, we compute the star formation rate (SFR) as

$$\frac{\text{SFR}}{M_\odot \, \text{yr}^{-1}} = \epsilon \times 0.0328 \left(\frac{M_{\text{cold,comp}}}{10^{11} \, M_\odot} \right)^{1.4} \left(\frac{R_{\text{comp}}}{1 \, \text{Mpc}} \right)^{-0.8}, \quad (1)$$

and we assume a Kennicutt IMF (Kennicutt 1983). $M_{\text{cold,comp}}$ and R_{comp} are, respectively, the mass of cold (i.e. neutral) gas in the ISM and the radius of each galaxy component: disc, bulge and burst (see Hatton et al. 2003, for details). ϵ is the star formation efficiency parameter.

Thirdly, we now compute extinction by dust using a simple screen model, which is consistent with our expanding shell scenario (see Section 3), and we introduce a redshift dependency in the dust-to-gas ratio. In practice, we follow Hatton et al. (2003) and write the dust optical depth as

$$\tau_{\text{dust}}(\lambda) = \left(\frac{A_\lambda}{A_V} \right)_{Z_\odot} \left(\frac{Z}{Z_\odot} \right)^{1.35} \left(\frac{N_H}{2.1 \times 10^{21}} \right) f(z), \quad (2)$$

where $(A_\lambda/A_V)_{Z_\odot}$ is the extinction curve for solar metallicity taken from Mathis, Mezger & Panagia (1983), Z is the metallicity of the absorbing gas (equal to that of the ISM), and N_H is the H I column density. We compute this latter quantity with equation (10), written for the expanding shell. It is worth noting, however, that because of our choice of parameters for the shell, equation (10) is very similar to that used in Hatton et al. (2003, equation 6.3). The last term in equation (2) introduces a scaling of the dust-to-gas ratio with redshift as $f(z) = (1 + z)^{-1/2}$. This scaling is in broad agreement with obervational results of e.g. Reddy et al. (2006), and has already been used in models, e.g. by Kitzbichler & White (2007). Finally, we compute the spectral energy distributions (SEDs) of our model galaxies with the STARDUST library (Devriendt, Guiderdoni & Sadat 1999), as in Hatton et al. (2003), and extinguish them using a screen model

$$L_{\text{obs}}(\lambda) = e^{-\tau_{\text{dust}}(\lambda)} L_{\text{intrinsic}}(\lambda). \quad (3)$$

Such a model allows us to be consistent both with the physical scenario we implement and with the absorption in the continuum found in the MCLYA library (see Section 3.2.1).

In order to adjust our model at high redshift, we want to be able to reproduce the UV LFs at $z \sim 3$, 4 and 5. To do so, we adjust the star formation efficiency parameter ϵ. $\epsilon = 1$ gives the Kennicutt law as observed at low redshifts. In this model, we need to adopt $\epsilon = 25$ to fit the UV LFs. Although this may seem extreme, some theoritical works suggest that indeed star formation is a more violent process at high redshifts (Somerville, Primack & Faber 2001). On the observational side, there are quite few estimates of the star formation efficiency at high redshift. Baker et al. (2004) measured the SFR and molecular gas density in a $z = 3$ LBG and found that the relation between them agrees with the $\epsilon = 1$ Kennicutt law. However, using their molecular gas density measurement at 1σ can yield $\epsilon = 5$. With a recent *WMAP*5 cosmology simulation, we find that GALICS can reproduce the UV LF between $z = 3$ and 5 with a star formation efficiency ϵ of only 5. We have checked that it has very little impact on the statistical properties of high-redshift galaxies in our model. More importantly, the results of the Lyα model remain fully consistent with those presented in this article. Therefore, we
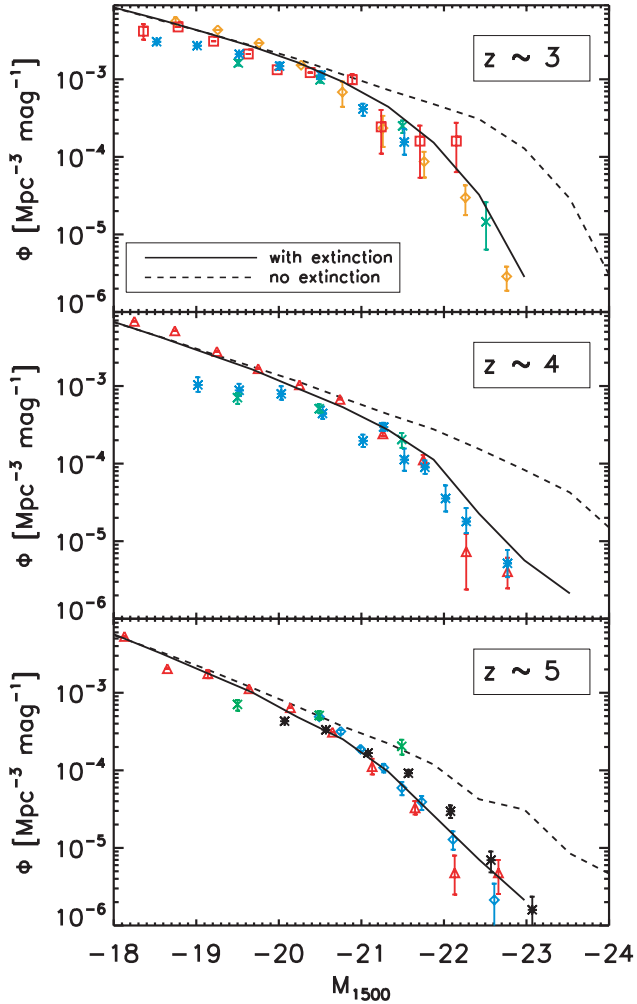
---

[2] http://www.projet-horizon.fr
[3] http://www.mpa-garching.mpg.de/gadget/

Figure 1. Absolute rest-frame UV LFs (at 1500 Å) at $z \sim 3$, 4 and 5. In each plot, the solid line refers to the UV LF after extinction while the dashed line represents the non-extinguished LF. Data points are from Reddy et al. (2008) (orange diamonds), Arnouts et al. (2005) (red squares), Sawicki & Thompson (2006) (blue asterisks), Gabasch et al. (2004) (green crosses), Bouwens et al. (2007) (red triangles), Iwata et al. (2007) (black asterisks) and McLure et al. (2009) (blue diamonds).

think that, even if it may appear as a strong deviation from local values, the high-redshift star formation efficiency we have used is not a serious problem, and can be decreased with simulation runs with an updated cosmology. These results will be presented in a next paper (Garel et al., in preparation). Also, and perhaps more importantly, the idea of this work is to use GALICS as a framework to explore the implications of our model for Lyα emission. In this prospect, it is only important for us here to have a model which reproduces somehow galaxy properties at high redshift.

In Fig. 1, we show the rest-frame UV LFs in a filter centred at 1500 Å, at $z \sim 3$, 4, and 5, with $\epsilon = 25$. In each panel, the solid line shows our predictions (including the effect of dust) and gives a good match to the observational data. The dashed line shows our predictions prior to extinction. The strong attenuation (~ 1 mag) we find at the bright end corresponds to the lower limit suggested by the analysis of LBGs (Pettini et al. 1998; Steidel et al. 1999; Blaizot et al. 2004).

We can now turn to investigating the Lyα properties of our high-redshift model galaxies.

3 LYα MODEL

One can write the Lyα luminosity $L_{\mathrm{Ly}\alpha}$ of a galaxy as

$$L_{\mathrm{Ly}\alpha} = L_{\mathrm{Ly}\alpha}^{\mathrm{intr}} \times f_{\mathrm{esc}}, \tag{4}$$

where $L_{\mathrm{Ly}\alpha}^{\mathrm{intr}}$ is the *intrinsic* Lyα luminosity, and f_{esc} is the fraction of these photons that actually escape the galaxy. The first term is dominated by recombinations from photo-ionized gas in H II regions, and we compute it in Section 3.1. The second term is the result from complex resonant radiative transfer. We present our model for f_{esc} in Section 3.2, and discuss its basic properties. In Section 3.3, for the sake of discussion and comparison, we present a selection of alternative models found in the literature.

The possible attenuation of the Lyα line by the IGM is discussed later (cf. Section 4.4).

3.1 Intrinsic Lyα luminosities

We compute the production rate of hydrogen-ionizing photons $Q(H)$ by integrating each galaxy's SED up to 912 Å. We then write the intrinsic Lyα luminosity as

$$L_{Ly\alpha}^{\mathrm{intr}} = \frac{2}{3} Q(H) \left(1 - f_{\mathrm{esc}}^{\mathrm{ion}}\right) \frac{hc}{\lambda_\alpha}, \tag{5}$$

where $\lambda_\alpha = 1216$ Å is the Lyα line centre, $f_{\mathrm{esc}}^{\mathrm{ion}}$ is the escape fraction of ionizing photons, c the speed of light, h the Planck constant, and the factor 2/3 comes from the case B recombination (Osterbrock 1989). Throughout this paper, we assume that galaxies are ionization-bound so that $f_{\mathrm{esc}}^{\mathrm{ion}} = 0$.

We assume the intrinsic Lyα line profile (Φ) to be a Gaussian centred on λ_α and with a width given by the rotational velocity v_{rot} of the sources in the gravitational potential of the galaxy

$$\Phi(\lambda) = \frac{c}{\sqrt{\pi}\, v_{\mathrm{rot}} \lambda_\alpha} e^{-\left[\frac{c(1-\lambda/\lambda_\alpha)}{v_{\mathrm{rot}}}\right]^2}. \tag{6}$$

The intrinsic Lyα equivalent width ($EW_{Ly\alpha}^{\mathrm{intr}}$) is simply

$$EW_{Ly\alpha}^{\mathrm{intr}} = \frac{L_{Ly\alpha}^{\mathrm{intr}}}{L_{1216}^{\mathrm{intr}}}, \tag{7}$$

where L_{1216}^{intr} is the unattenuated continuum luminosity estimated by integrating each galaxy's SED from 1200 to 1230 Å.

3.2 Fiducial radiative transfer model

In our model, the Lyα line properties are determined by resonant scattering through a gas outflow. In practice, we compute the Lyα line properties for each model galaxy as a post-processing step of GALICS as follows. First, we follow Verhamme et al. (2008) and model the gas outflow as an expanding shell of neutral gas and dust. We relate the shell parameters to each model galaxy's physical properties in Section 3.2.2. Second, we use the Schaerer et al. (2011) numerical library to derive accurately the Lyα profile and escape fraction for each galaxy.

Here, we briefly present this library, and then describe the shell model we assume for each galaxy.

3.2.1 MCLYA *library*

Schaerer et al. (2011) have extended the work of Verhamme et al. (2008) by constructing a library of numerical experiments in which they compute the transfer of Lyα photons from a central source through an expanding (or static) spherical, homogeneous shell of

Table 2. Grid of parameters used from the MCLYA library of Schaerer et al. (2011), assuming $b = 20\,\mathrm{km\,s^{-1}}$.

$V_{\mathrm{exp}}(\mathrm{km\,s^{-1}})$	0	20	50	100	150	200	250	300	400	500	600	700
$\log N_{\mathrm{H}}$	16	18	18.5	19	19.3	19.6	19.9	20.2	20.5	20.8	21.1	21.4	21.7
τ_{dust}	0	0.001	0.1	0.2	0.5	1	1.5	2	3	4		

mixed H I and dust. In their model, a shell is described by four parameters: its expansion velocity V_{exp}, its H I column density N_{H}, its dust opacity τ_{dust} and the velocity dispersion of the gas within the shell b. The library constructed by Schaerer et al. (2011) explores a wide range of these parameters, which we summarize in Table 2, and consists of more than 5000 models. Note that for simplicity, we have fixed one parameter (b) to a constant value of $b = 20\,\mathrm{km\,s^{-1}}$ (which corresponds to a typical gas temperature $T \sim 10^4\,\mathrm{K}$). This choice is motivated both by the fact that Verhamme et al. (2006) have shown this parameter to have the least impact on their results, and by the fact that there is no clear physical way to vary this parameter for each of our galaxies.

In each experiment, photons are emitted from the central source with frequencies ranging from -6000 to $+6000\,\mathrm{km\,s^{-1}}$ around the Lyα line.

This extent, which has been chosen in Schaerer et al. (2011) to compute the grid of models, is almost always sufficient to cover the whole frequency range where resonant effects play a role.

For each experiment, the library contains the escape fraction and the observed wavelength distribution of escaping Lyα photons as a function of their input wavelength. Far from the line centre, the library also predicts extinction of the continuum by dust, and gives results consistent with our equation (3).

In very few extreme cases [less than one object out of a thousand at any redshift, corresponding to $\log(N_{\mathrm{H}}) > 21.4$ and $\tau_{\mathrm{dust}} > 2$], the expanding shells produce very damped absorption lines blueward 1216 Å, with extended wings which can contribute up to 25 per cent extra extinction at $6000\,\mathrm{km\,s^{-1}}$, compared to the non-resonant prediction of equation (3). In these cases, the MCLYA library does not allow us to compute accurately the Lyα EW (equation 11). However, all these galaxies have a Lyα EW < 0 Å and luminosity $<10^{42}\,\mathrm{erg\,s^{-1}}$, which is less than the selection criteria of observations we compare our results with. We have checked that increasing or reducing by an arbitrary 30 per cent the EW of the very few galaxies in such a configuration does not change our results in any notable way.

From this library, we can compute an emergent spectrum for each model as

$$S(\lambda) = \sum_i [C(\lambda_i) + \Phi(\lambda_i)] \times f_{\mathrm{esc}}^i \times \phi_{\mathrm{out}}^i(\lambda), \qquad (8)$$

where the sum extends over emission wavelengths λ_i, C is the stellar continuum prior to extinction, Φ is the input line profile (equation 6), f_{esc}^i is the fraction of photons emitted at λ_i which escape the shell and ϕ_{out} is their normalized wavelength distribution. Both C and Φ are predicted from GALICS (Sections 2.2 and 3.1), and the library gives us values for f_{esc} and ϕ_{out} for each shell model. The full coupling with GALICS thus requires one more step: the prediction of the shell parameters which will allow the selection of the appropriate MCLYA model for each galaxy.

In practice, we will need to interpolate our predicted shell parameters (V_{exp}, N_{H} and τ_{dust}) between grid points provided by the MCLYA library. The V_{exp} grid is interpolated linearly whereas we use a logarithmic interpolation for N_{H} and τ_{dust} (it is due to the fact that f_{esc} values evolve rapidly with N_{H} and τ_{dust} compared to V_{exp}). Also,

some of the parameter values predicted by GALICS are found to be outside the available MCLYA grid, in which case we simply adopt the model at the corresponding boundary.

The number of these outliers is small compared to the whole sample [$\sim$6000 over more than 1 million (400 000) at $z = 3.1$ (4.9)]. There are no objects with $V_{\mathrm{exp}} > V_{\mathrm{exp}}^{\mathrm{grid,max}}$. Objects with $\tau_{\mathrm{dust}} > \tau_{\mathrm{dust}}^{\mathrm{grid,max}}$ (a few hundreds at any redshift) are already very faint LAEs ($L_{\mathrm{Ly}\alpha} < 10^{41}\,\mathrm{erg\,s^{-1}}$) when we attribute them the value $\tau_{\mathrm{dust}}^{\mathrm{grid,max}}$. They would be even fainter with their *true* dust opacity value, and then fall below the luminosity limit we are interested in this study. Galaxies displaying a shell column density higher than $N_{\mathrm{H}}^{\mathrm{grid,max}}$ are the most numerous (a few thousands at any redshift). All of them have Lyα luminosity $L_{\mathrm{Ly}\alpha} < 5 \times 10^{42}\,\mathrm{erg\,s^{-1}}$ and an EW less than 30 Å. Making the calculation with their *real N_{H}* value would tend to reduce even more their escape fraction (and consequently their Lyα luminosity and EW). We did the extreme test of setting all the Lyα luminosities of the outliers to zero and found that it does not affect the results and conclusions of the paper.

3.2.2 Shell model

In order to make use of the MCLYA library described above, we now need to derive the shell parameters (expansion velocity, column density and dust opacity) for each model galaxy. We do this as a post-processing step[4] of the GALICS run, by using simple scaling arguments as follows.

First, we use a prescription taken from Bertone, Stoehr & White (2005) for the shell velocity (see also Shu, Mo & Shu-DeMao 2005)

$$V_{\mathrm{exp}} = 623 \left(\frac{\mathrm{SFR}}{100\,\mathrm{M_\odot\,yr^{-1}}} \right)^{0.145}\,\mathrm{km\,s^{-1}}, \qquad (9)$$

which links the speed of the outflowing gas to the SFR of the galaxy.

Second, we need to estimate the size and the gas mass of shell to describe its column density. We assume the shell radius is of the order of the disc radius R and we take $R_{\mathrm{shell}} = R$, where $R \sim \lambda R_{\mathrm{vir}}/\sqrt{2}$, with λ the spin parameter and R_{vir} the virial radius of the host halo (see Hatton et al. 2003, for details). We have checked that integrating the amount of ejected gas over a few Myr typically gives a mass of the same order as that present in the ISM. For the sake of simplicity, we decide to set $M_{\mathrm{shell}}^{\mathrm{gas}} = M_{\mathrm{cold}} = \sum_{\mathrm{comp}} M_{\mathrm{cold,comp}}$ (the total mass of cold gas in the galaxy).

We can now compute the shell H I column density as

$$N_{\mathrm{H}} = \frac{M_{\mathrm{shell}}^{\mathrm{gas}}}{4\pi \mu m_{\mathrm{H}} R^2}\,\,\mathrm{atoms\,per\,cm^2}, \qquad (10)$$

where m_{H} is the hydrogen atom mass and μ is the mean particle mass in a fully neutral gas ($\mu = 1.22$).

Finally, we compute the shell's dust optical depth at 1216 Å using equation (2). Note that the models for the H I column density and dust opacity are identical for the Lyα and the UV continuum

---

[4] Note that this shell model is done in post-processing, not in GALICS, so that it has no impact on the subsequent gas evolution and star formation in the GALICS run.

calculations. This implies that the continuum extinction seen in the spectra from the MCLYA library matches the extinction that we apply to our galaxy SEDs. This match allows us to build full spectra for each model galaxy, and to measure the Lyα EW directly as

$$\mathrm{EW}_{\mathrm{Ly}\alpha} = \int \frac{S(\lambda) - C_{\mathrm{ext}}(\lambda)}{C_{\mathrm{ext}}(\lambda)} \mathrm{d}\lambda, \tag{11}$$

where S is defined in equation (8) and C_{ext} is the extinguished stellar continuum.

3.2.3 Shell parameters distributions

In Fig. 2, we show our predicted distributions of the three shell parameters at $z = 3.1$ and 4.9 (they are similar at other redshifts). These quantities show expected correlations. First, there is a tight positive correlation between N_{H} and τ_{dust}, which directly results from our assumption that $\tau_{\mathrm{dust}} \propto N_{\mathrm{H}}$ in equation (2). The small scatter across this relation is due to metallicity. Second, the shell velocity is a (weak) function of the SFR. Galaxies with more active star formation have a larger reservoir of cold gas, and hence faster shells are also those with higher H I column densities. The linear relation between N_{H} and τ_{dust} is responsible for the similar behaviour in the $V_{\mathrm{exp}} - N_{\mathrm{H}}$ and $V_{\mathrm{exp}} - \tau_{\mathrm{dust}}$ planes.

At all z, the H I column density goes from $\sim 10^{16}$ to a bit less than 10^{24} cm^{-2}. The most probable value of N_{H} is $\sim 10^{20}$ (5×10^{20}) cm^{-2} at $z = 3.1$ (4.9). The shell velocity distributions span a whole range of values from a few tens to 650 km s^{-1}. Most of the galaxies have $V_{\mathrm{exp}} \sim 150$–$200$ km s^{-1} which is consistent with the $z = 3$ sample of LBGs observed by Shapley et al. (2003). The dust opacity of the shells ranges from $\log(\tau_{\mathrm{dust}}) = -5$ to ~ 1.5. The peak of the distribution shifts from -2.5 at $z = 3.1$ to -2 at $z = 4.9$.

3.3 Other models for Lyα emitters

For discussion, we present here a selection of alternative models taken from the literature.

3.3.1 Constant f_{esc} model

The so-called *constant Lyα escape fraction* model, assumes a unique escape fraction of Lyα photons for all galaxies. Using such a model, Le Delliou et al. (2006) fit the Lyα LF data from $z = 3.3$ to 6.55 with a single value $f_{\mathrm{esc}} = 0.02$. On the other hand, Nagamine et al. (2010) obtain a reasonable fit to the data by varying f_{esc} with redshift, from 0.10 at $z = 3$, to 0.15 at $z = 6$.

Here, we chose a value of $f_{\mathrm{esc}} = 0.20$, which allows us to reproduce intermediate luminosity counts of the Lyα luminosity function at $z = 3.1$. This is also the largest value for our model not to over-predict the bright end of the LF.

For comparison, we also explore the extreme model in which all the Lyα photons are allowed to escape the galaxies, i.e. $f_{\mathrm{esc}} = 1$. In the next sections, we will refer to this model as the *no extinction* model.

3.3.2 Screen model

In the *screen* model, the fraction of Lyα photons that escape the galaxy is given by

$$f_{\mathrm{esc}} = \mathrm{e}^{-\tau_{\mathrm{dust}}}, \tag{12}$$

where τ_{dust} is the dust opacity of the shell. This means that the Lyα line is treated as a normal (non-resonant) radiation, Lyα photons see a *screen* of gas mixed with dust along their path. A similar model
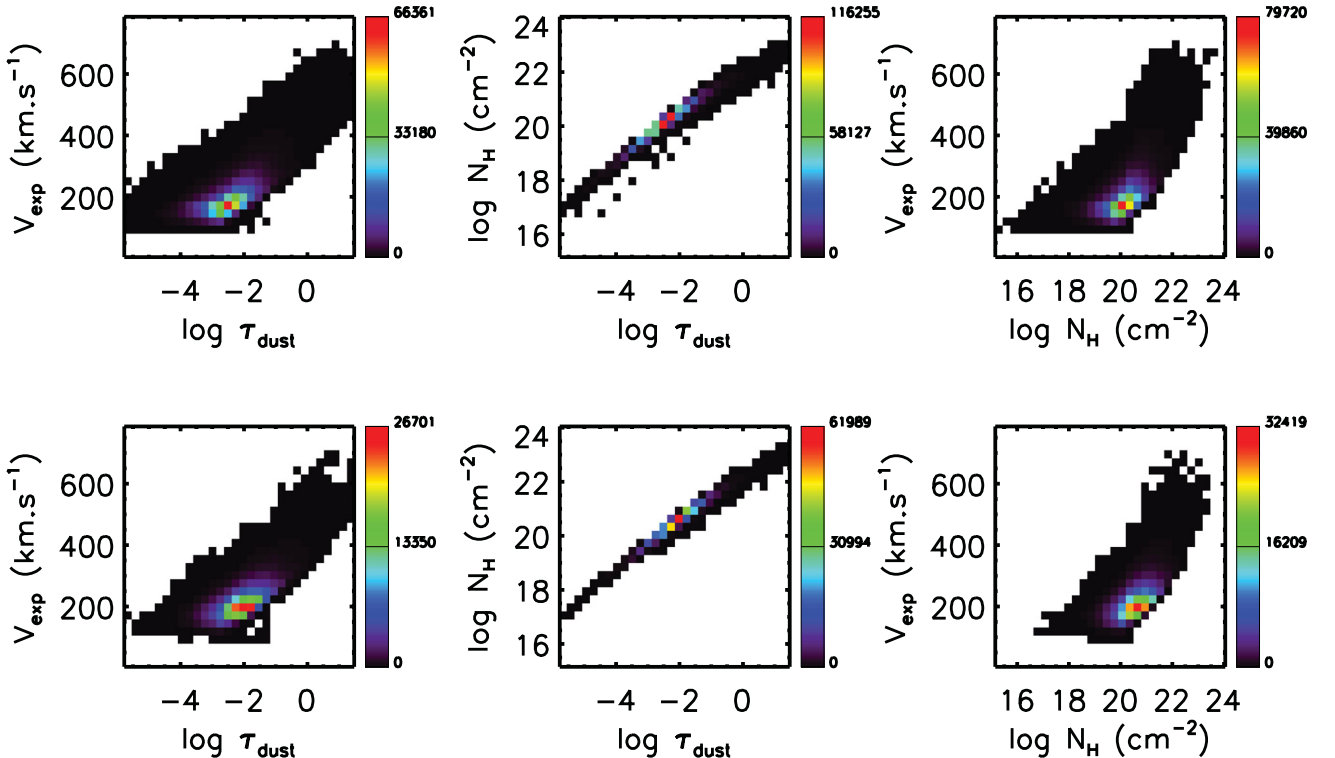

Figure 2. Correlations between the three shell parameters at $z = 3.1$ (upper panels) and 4.9 (lower panels) for the whole sample of galaxies. The expansion velocity V_{exp} is in km s^{-1} and the H I column density in cm^{-2}. τ_{dust} is the dust opacity evaluated at 1216 Å. The colour code scales with the number of objects in each pixel.

has been investigated by Kobayashi et al. (2007) and Mao et al. (2007) but these authors introduced an additional (free) parameter to reproduce the Lyα LF data.

3.3.3 Slab model

The *slab* model (Kobayashi et al. 2007), in which the escape fraction is

$$f_{esc} = \frac{(1 - e^{-\tau_{dust}})}{\tau_{dust}}, \tag{13}$$

is similar to the *screen* model, except that it assumes sources are no longer behind a screen, but uniformly distributed within a slab of gas mixed with dust. Again, and in contrast with us, Kobayashi et al. (2007, 2010) multiplied the above f_{esc} with a constant escape fraction f_0. These authors specify that this constant parameter f_0 takes into account the resonant scattering effect of Lyα photons, the escape of ionizing photons and the IGM transmission.

4 PREDICTED LYα ESCAPE FRACTIONS AND LYα LUMINOSITY FUNCTIONS

One of the strengths of our fiducial model is that it predicts the Lyα escape fraction of each individual galaxy, as a function of its physical properties. In this section, we first discuss our predicted Lyα escape fraction distribution. Then, we compare our predicted Lyα LFs to observational estimates. We continue with discussions on the EW selection effects and IGM attenuation.

4.1 Distribution of Lyα escape fractions

In Fig. 3, we show the distribution of f_{esc} for galaxies in different SFR bins, at $z = 3.1$ (thick curves) and $z = 4.9$ (thin curves).

A first point illustrated by Fig. 3 is that our model predicts a very strong variation of the escape fraction distribution with SFR (or,
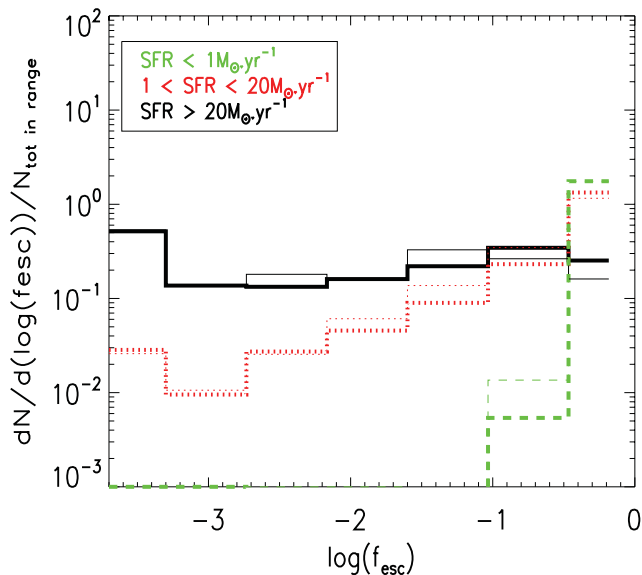
Figure 3. Distribution of Lyα escape fraction at $z \sim 3$ (thick line) and 5 (thin line). The black solid line refers to galaxies having SFR $> 20\,M_\odot\,yr^{-1}$, the red dotted line to $1 < SFR < 20\,M_\odot\,yr^{-1}$ and the green dashed one to low-SFR objects (SFR $<1\,M_\odot\,yr^{-1}$). Low-SFR galaxies have high Lyα escape fractions whereas in intensely star-forming objects, f_{esc} is distributed between 0 and 1.

equivalently, with stellar mass). We see that galaxies with high SFRs have a rather uniform f_{esc} distribution (solid black curves), while low-SFR objects let almost all Lyα photons escape (dashed green curves). The main quantity responsible for the flat distribution of the escape fraction for high-SFR galaxies is dust opacity. Galaxies with SFR $> 20\,M_\odot\,yr^{-1}$ span a τ_{dust} range going from 10^{-2} to more than 10, as a consequence of their different star formation and merging histories. Low-SFR objects contain little metal and H I gas. Consequently, their optical thicknesses are low, and their escape fractions high.

We find that the average (median) escape fraction for galaxies with SFR $> 10\,M_\odot\,yr^{-1}$ is 21 per cent (8 per cent). This compares nicely to the value of 20 per cent we used to fit our *constant Lyα escape fraction* model at intermediate Lyα luminosity ($10^{42} < L_{Ly\alpha} < 10^{43}$ erg s^{-1}).

A second point we wish to make from Fig. 3 is that the distribution of escape fractions, in a given SFR bin, remains almost constant with redshift. The fraction of galaxies per SFR bin does not change significantly between $z = 3$ and 5, because, from equation (1), the variations (that is, a decrease with increasing redshift) of cold gas mass and disc radius balance one another. In a given SFR bin, the values of H I column density and dust opacity (equations 10 and 2) remain rather similar over this redshift interval, as a result of the co-evolution of cold gas mass, disc radius and metallicity. This yields the apparent non-redshift evolution of Fig. 3.

4.2 Lyα luminosity functions

In Fig. 4, we show the observed Lyα luminosity functions from $z = 3.1$ to 4.9, and compare them to our model (solid black curves). Our model shows a very satisfactory agreement with the observational data over the whole redshift range. Interestingly, it fits as well the bright end ($L_{Ly\alpha} > 10^{42}$ erg s^{-1}) and the faint LAE population observed by Rauch et al. (2008) at $z \sim 3$. This is a direct result of our predicted escape fraction distribution. On the one hand, low-SFR galaxies have $f_{esc} \sim 1$ due to their low dust opacities, which allows us to reproduce the faint counts of Rauch et al. (2008). On the other hand, high-SFR galaxies have a flat distribution of f_{esc}, which yields the exponential cut-off at the bright end of the LF, as most of them have a very low escape fraction.

We note that, at $z = 3.1$, our model agrees better with spectroscopic observations (Kudritzki et al. 2000; van Breukelen et al. 2005; Rauch et al. 2008; Blanc et al. 2011) than with narrow-band data from Ouchi et al. (2008). We will come back to this issue in Section 4.3.

Fig. 4 also shows predictions of the other models discussed in Section 3.3. the blue dot–dashed (red dashed) curves show predictions from the $f_{esc} = 1$ ($f_{esc} = 0.20$) model, the blue long-dashed (green 3 dot–dashed) curves show predictions from the slab (screen) models. Interestingly, most models (all except the $f_{esc} = 0.20$ one) converge to the same faint-end prediction, consistent with $f_{esc} \sim 1$ for low-mass galaxies. Only our model, though, manages to also reproduce the bright end, due to its resonant scattering enhancing Lyα absorption in massive, dusty, galaxies.

At the faint end of the Lyα LFs where $f_{esc} \sim 1$, the Lyα luminosity could provide information about the SFR of low mass galaxies, assuming a standard conversion law (Kennicutt 1998; Furlanetto et al. 2005).
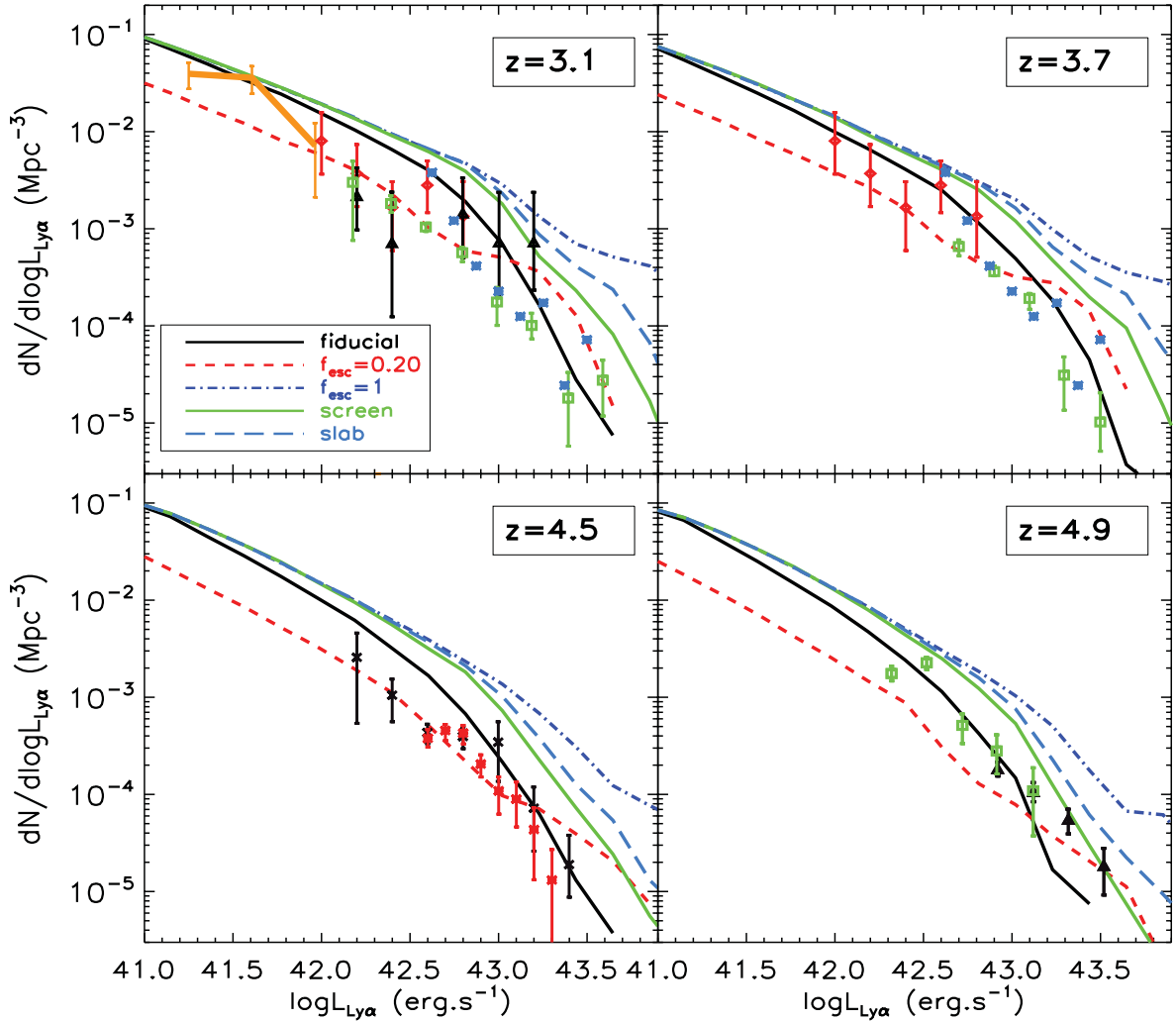
Figure 4. Lyα LFs at $z = 3.1, 3.7, 4.5$ and 4.9. Black solid line: fiducial model. Red short dashed line: $f_{esc} = 0.20$. Blue long dashed line: slab model. Violet dot–dashed line: $f_{esc} = 1$. Green dot–dot–dashed line: screen model. The data points are from van Breukelen et al. (2005) (red diamonds, $2.3 < z < 4.6$), Kudritzki et al. (2000) (black triangles, $z = 3.1$), Ouchi et al. (2008) (green squares, $z = 3.1, 3.7$), Blanc et al. (2011) (blue asterisks, $2.8 < z < 3.8$), Dawson et al. (2007) (black crosses, $z = 4.5$), Wang et al. (2009) (red asterisks, $z = 4.5$), Ouchi et al. (2003) (green squares, $z = 4.9$) and Shioya et al. (2009) (black triangles, $z = 4.9$). The orange line is the observation of Rauch et al. (2008) ($2.67 < z < 3.75$).

4.3 Selection effects

Let's note that data from Ouchi et al. (2008) (which represents the largest sample of LAEs) around $\log(L_{Ly\alpha}) \sim 42.1–42.8$ are a bit overestimated by our model. The theoretical Lyα LFs presented in Fig. 4 do not contain any kind of selection effect. However, when selected through narrow-band searches, as in Ouchi et al. (2008), observations are subject to a threshold in terms of Lyα EW. Ouchi et al. (2008), especially, have a relatively high threshold at $z = 3.1$ ($EW^{thresh} \sim 64$ Å). Since our model is able to predict the emergent Lyα EW of LAEs, we can reproduce such a selection and investigate its impact on LFs estimates.

In Fig. 5, we focus on the Lyα LF at $z = 3.1$ and show how it varies when selecting galaxies with increasing EWs. The solid curve is the same as in Fig. 4 (no selection), the dotted (dashed, dot–dashed) curves correspond to cuts at 35 Å (50 Å, 64 Å). Fig. 5 shows that a selection on EW affects the LF *at all luminosities*, in a rather uniform way. Even at low luminosities ($<10^{41}$ erg s^{-1}), our model galaxies have a distribution of EWs peaking at around ~ 65 Å, and are thus affected by drastic EW cuts.

When using the threshold value of 64 Å quoted by Ouchi et al. (2008) at face value, we find that our model underpredicts the number density of LAEs observed by these authors (green open squares in Fig. 5). Instead, we find good agreement with their LF when applying a cut at ~ 50 Å. We believe this discrepancy has two causes: (i) our distribution of predicted EWs is perhaps centred at too low values and (ii) there is a rather large uncertainty in the estimated value of the effective EW cut from these authors' survey. We discuss our predictions for EWs again in Section 5.1.

We learn from this study that narrow-band observations may underestimate the actual number density of LAEs at all luminosities, by a factor ranging from 5 at the bright end to ~ 2 at the very faint end ($L \sim 10^{41}$ erg s^{-1}). Spectroscopic surveys, which are much less sensitive to EW thresholds, are more efficient to detect the whole sample of LAEs. Indeed, it can be seen from Fig. 4 that most data points obtained by spectroscopy (Kudritzki et al. 2000; van Breukelen et al. 2005; Blanc et al. 2011) are most of the time above Ouchi et al. (2008) observations, and in better agreement with our model predictions. However, comparing with Gronwall et al. (2007) data (who have a much lower EW limit, i.e. 20 Å) does not lead
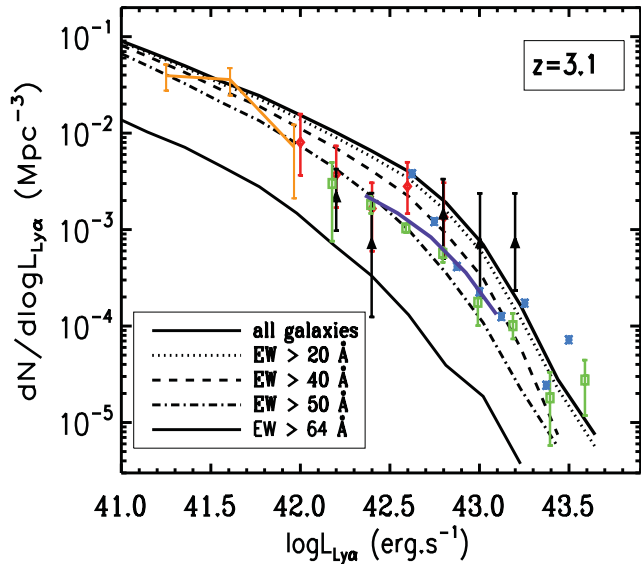
Figure 5. Impact of a Lyα EW threshold on the Lyα LF at $z = 3.1$. We plot five LFs with different cuts in Lyα EW. Solid line: no cut. Dotted line: EW$^{\text{thresh}}$ > 20 Å. Dashed line: EW$^{\text{thresh}}$ > 35 Å. Dot–dot–dashed line: EW$^{\text{thresh}}$ > 50 Å. Dot–dashed line: EW$^{\text{thresh}}$ > 64 Å. Data points are the same as in Fig. 4. Gronwall et al. (2007) data are shown as a thick violet line.

to the same conclusion. Gronwall et al. (2007) data (blue dashed line) are very close to those from Ouchi et al. (2008). Applying the 20 Å to our fiducial model does not reproduce their observed Lyα LF. Understanding why both Ouchi et al. (2008) (sample of 356 objects) and Gronwall et al. (2007) (sample of 162 objects) give a very similar luminosity function at $z = 3.1$ despite of quite different EW limits is not straightforward, given that the number of LAEs detected with EW <64 Å is not negligible (Finkelstein et al. 2007; Gronwall et al. 2007). It may be a cosmic variance effect.

In the next paragraph, we discuss what limitations arise from spectroscopic observations we have compared our model with and for which our Lyα LF shows a better match than with narrow-band data.

Observations of Kudritzki et al. (2000) were carried out with slit spectroscopy over ∼50 arcmin^2 so that their results may be biased by flux losses and cosmic variance. Low redshift interlopers may also have been identified as LAEs. Blanc et al. (2011) apply a 20 Å EW cut to remove O II emitters from their sample. According to our Fig. 5, such a low EW threshold should remove a small fraction of LAEs only. Integral field spectroscopy data from van Breukelen et al. (2005) cannot distinguish O II emitters so that their sample of LAEs may be considered as a *maximal* sample. They argue that 2 LAEs from their sample could be O II emitters. We did the test of removing those two objects which lie in the two *brighter* bins of their LF. We found that our model is still in good agreement with these two points even after this correction. Nevertheless, the field of view of van Breukelen et al. (2005) is rather small (∼1.4 arcmin^2) and their data may suffer of cosmic variance effects. A more detailed discussion on pros and cons of narrow-band techniques versus integral field spectroscopy or slit spectroscopy is postponed to a future study (Garel et al., in preparation).

Finally, we note that EW limits of narrow-band surveys have a decreasing effect with redshift (see Table 3), so that the number of objects found with narrow-band and spectroscopic techniques should converge at higher redshifts.

Table 3. Detection limits of narrow-band surveys.

Author	Redshift	EW$_{\text{Lyα}}$[a] (Å)	$L_{\text{Lyα}}$[b] (erg s^{-1})
Ouchi et al. (2008)	$z \sim 3.1$	64	10^{42}
Gronwall et al. (2007)	$z \sim 3.1$	20	1.1×10^{42}
Ouchi et al. (2008)	$z \sim 3.7$	44	4×10^{42}
Dawson et al. (2007)	$z \sim 4.5$	14	4×10^{42}
Finkelstein et al. (2007)	$z \sim 4.5$	20	4×10^{42}
Wang et al. (2009)	$z \sim 4.5$	14	3.5×10^{42}
Ouchi et al. (2003)	$z \sim 4.9$	14	7×10^{41}
Shioya et al. (2009)	$z \sim 4.9$	11	3.8×10^{42}

[a]Limiting Lyα rest-frame EW of the survey.
[b]Limiting Lyα luminosity of the survey.

4.4 Effect of the IGM

In the results presented so far, we have not included the effect of IGM transmission. However, photons shortwards 1216 Å may be scattered off the line of sight by intergalactic hydrogen atoms. We model this effect as Madau (1995), and define the IGM optical depth as

$$\tau_{\text{IGM}}^{\text{Lyα}} = 0.0036 \left(\frac{\lambda_{\text{obs}}}{\lambda_\alpha} \right)^{3.46}, \tag{14}$$

where $\lambda_{\text{obs}} = (1 + z)\lambda$ is the observer-frame wavelength.

We apply the IGM transmission $T_{\text{IGM}}^{\text{Lyα}} = e^{-\tau_{\text{IGM}}^{\text{Lyα}}}$ to the blue part of our spectra, only in the fiducial model (in which we build the emergent Lyα spectra) and in the *no extinction* model (where we assume the spectrum is unchanged compared to the Gaussian intrinsic spectrum). Other models do not produce spectra and so we discard them here. Note that if one assumes that the $f_{\text{esc}} = 0.20$ model does not affect the line shape but only its amplitude, it would undergo exactly the same IGM attenuation as the *no extinction model* does.

In Fig. 6, we show how the IGM transmission affects the Lyα LF at 3.1 and 4.9 only since the results at $z = 3.7$ and 4.5 lead to the same conclusions we discuss below. We find that the IGM has a negligible impact on our model's Lyα LFs. This is due to the fact that, in this model, most of the galaxies' spectra have P-Cygni profiles, with a redward peak in emission and a deep absorption on the blue side. As our model for IGM transmission only applies to the blue side of the spectra, we indeed expect little effect from the IGM. This is probably a good approximation in most cases where the IGM does not produce any damped absorption line which could leak redwards of the Lyα line. The fact that the attenuation of Lyα by the IGM may be relatively small or even negligible in the case of outflows has already been noted by several authors, including e.g. Haiman (2002), Santos et al. (2004), Verhamme et al. (2008), Dijkstra & Wyithe (2010) and others. In the *no extinction* model, we have assumed the spectra emerging from the galaxy are Gaussian. In this case, the transmission through the IGM has a clear effect on the LF: it reduces luminosities by a factor ∼2 at $z = 5$. This is not enough, however, to bring this model in agreement with the data at $z \leq 5$, which suggests that IGM attenuation alone cannot explain the observations.

5 PROPERTIES OF LYα EMITTERS

We now study in more detail the properties of LAEs at $3 < z < 5$ as predicted by our fiducial model, and we compare them to other available data.
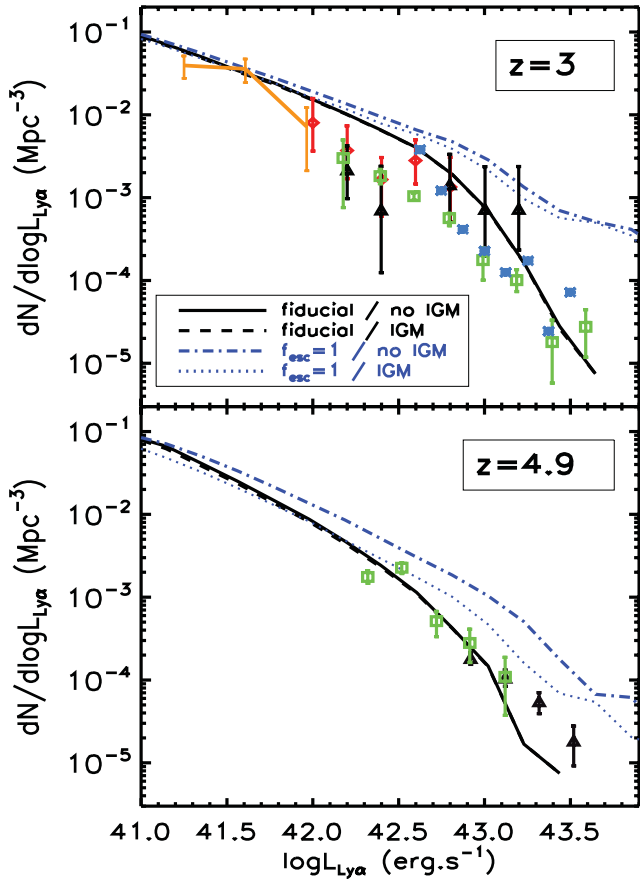
Figure 6. Comparison of the Lyα LFs at $z = 3.1$ and 4.9 with and without IGM transmission. The behaviour is similar at $z = 3.7$ and 4.5. Black solid line: fiducial model without IGM. Black dashed line: fiducial model with IGM. Violet dot–dashed line: No extinction model without IGM. Violet dotted line: No extinction model with IGM. Note that a horizontal shift of $\log(0.20)$ of the violet curve gives the $f_{esc} = 0.20$ model in the assumption that the line shape is unchanged by shell transfer effects. Data points are the same as in Fig. 4.

5.1 Lyα equivalent width

In this section, we present the rest-frame intrinsic Lyα EWs obtained from equation (7), and the rest-frame emergent (after radiation transfer) Lyα EWs predicted by our fiducial model from equation (11).

In Fig. 7, we compare our predicted Lyα EW distributions with observations at various redshifts ($z = 3.1, 3.7, 4.5$ and 4.9). To perform a reliable comparison, we apply the same criteria in terms of Lyα luminosity and EW cuts as in each data set (see Table 3). In each panel, we show three histograms. The dotted green curve represents the raw distribution of intrinsic Lyα EWs. The peak is at 65–70 Å at all redshifts, with very few objects having high Lyα EWs (>100 Å). The first reason of the deficit of high Lyα EWs, and of the absence of very high Lyα EWs (>200 Å) may be the absence of star formation bursts in our GALICS galaxies. Indeed, as gas accretion is a continuous and smooth process, the SFRs evolve smoothly and no galaxies show very short time-scale bursts able to enhance the Lyα EW. Galaxies displaying a constant SFR have rather low Lyα EWs (Charlot & Fall 1993). Another reason for our lack of high EWs may be that we use a Kennicutt IMF. Considering a shallower IMF, or a higher high-mass cut-off could enhance the intrinsic Lyα EWs (Charlot & Fall 1993). A third reason for the

shallow distribution of emergent EWs could be due to large errors in the estimate of EWs. To take into account statistical uncertainties, we have convolved this distribution with a Gaussian ($\sigma = 50$ Å), which yields the green dashed curve. The choice of 50 Å is arbitrary and corresponds to the size of the bin in Fig. 7 and in the Lyα EWs distributions commonly presented by observers. We assume that the dispersion in measurement uncertainties should not exceed this value (though it is hard to quantify). Even with this 'high' σ value, we do not reach very high intrinsic Lyα EWs (>200 Å).

We do not show the raw distribution of emergent Lyα EWs obtained with our model for the sake of clarity. At $z = 3.1$–3.7, it is hardly distinguishable from the intrinsic distribution. At $z = 4.5 - 4.9$, the peak would be shifted to the 0–50 Å bin and the distribution as narrow as the raw distribution. In Fig. 7, the solid black line represents the distribution of emergent Lyα EWs convolved with a Gaussian ($\sigma = 50$ Å), as we did for the intrinsic distribution. We can see that, at $z = 3.1, 3.7$ and 4.9, the locations of the peaks of the distributions in our predictions are in agreement with the observations. We should note that, at $z = 4.5$, even if the model peak matches the observed distribution from Finkelstein et al. (2007), it is not the case compared with Dawson et al. (2007) data. However, if we were comparing this $z = 4.5$ model distribution with $z = 4.9$ data from Shioya et al. (2009), we would get a good match (Dawson et al. 2007; Finkelstein et al. 2007; Shioya et al. 2009, have nearly the same luminosity and EW detection limits so the same model can compare with these observations). Then, we argue that it is hard to draw conclusions in that case. On the other hand, it is straightforward to conclude that all our distributions are not spread enough compared with any data. We discuss briefly this issue.

The emergent Lyα EWs obtained with our fiducial model are lower than the intrinsic ones which, as discussed above, do not reach large values and have a narrow distribution. Since the amount of dust seen by the continuum and the Lyα line is the same, and given that the Lyα line is resonant (and, consequently, more extinguished), it is impossible for any galaxy to have an emergent Lyα EW greater than the intrinsic one in our model. Only models with clumpy dust distributions (Neufeld 1991) would allow $EW_{Ly\alpha} > EW_{Ly\alpha}^{intr}$. Despite the lack of large EW systems, we note that our distribution reproduces a significant fraction of observed systems, which is satisfactory.

The reproduction of a shallow Lyα EW distribution with very large Lyα EWs is a puzzling issue for other models too (Dayal et al. 2008; Samui et al. 2009). Dayal et al. (2008) argue that physical effects such as gas kinematics, metallicity, Population III stars and young stellar ages could spread the EW distribution, and lead to higher EW values. Kobayashi et al. (2010) are able to retrieve the very large Lyα EWs thanks to the inclusion of both young and low-metallicity stellar populations and clumpy dust in their time-sequence outflow model. The value of their *clumpiness parameter* ($q_d = 0.15 = $ clumpy dust) arises from the calculation of both continuum and Lyα dust opacities which are computed from two different ways.

5.2 UV luminosity functions of Lyα emitters

As noted in Samui et al. (2009), only a fraction of the whole galaxy population is detected as LAEs because of the survey limits (in $L_{Ly\alpha}$ and EW). By applying the same thresholds as in the observations, we compute the UV LFs of LAEs at $z = 3.1, 3.7$ and 4.9 with our fiducial model and investigate the relation between UV-selected galaxies (LBGs) and LAEs.
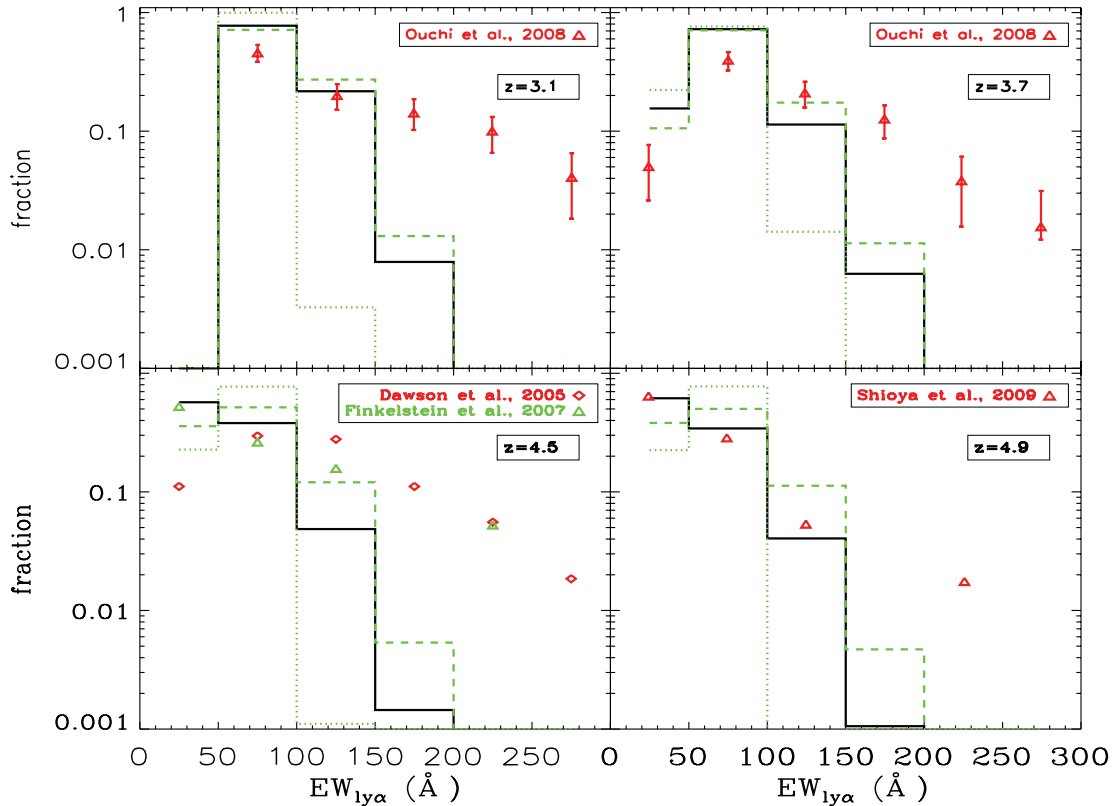
Figure 7. EW distributions at $z = 3, 3.7, 4.5$ and 4.9. Dotted green line: raw distribution of intrinsic Lyα EWs. The two other curves have been convolved with a Gaussian ($\sigma = 50$ Å) to account for statistical uncertainties. Solid black line: emergent Lyα EW distribution (fiducial model) with convolution. Dashed green line: intrinsic Lyα EW distribution with convolution. We apply the same thresholds in terms of Lyα EW and luminosity as each individual set of data as summarized in Table 3.
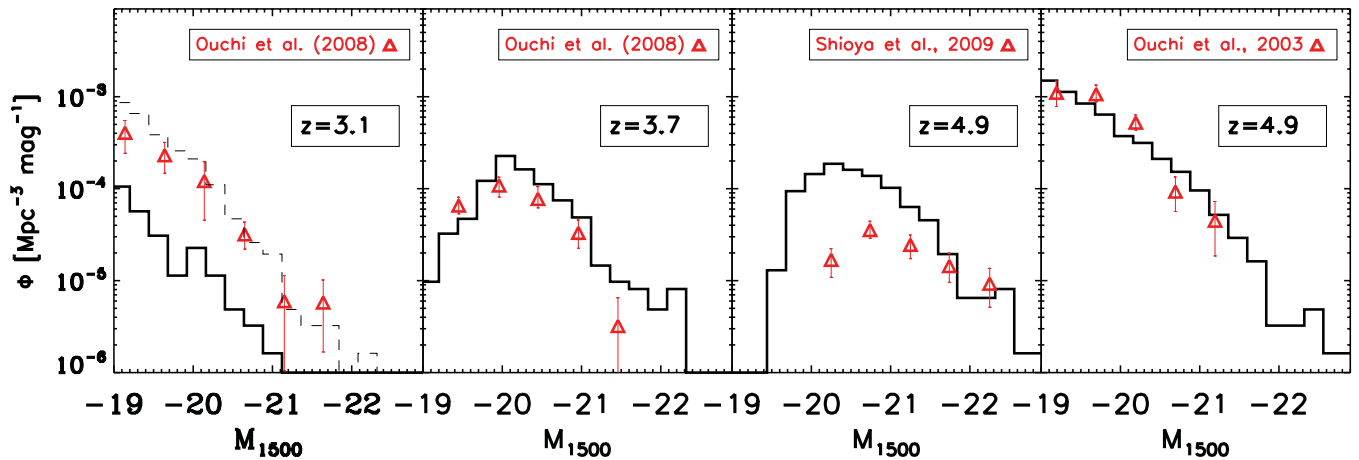
Figure 8. Observed (red symbols) and predicted (black lines) rest-frame UV LFs of LAEs at 1500 Å. For each LF, we apply the same cuts in Lyα luminosity and EW as in the observations. The dashed line at $z \sim 3.1$ (left-hand panel) shows the model applying a somewhat lower EW threshold of 50 Å.

In Fig. 8, we show the UV LFs of Lyα-selected model galaxies. We find a rather good agreement with observations, especially with Ouchi et al. (2008) at $z = 3.7$, and with Ouchi et al. (2003) at $z = 4.9$. However, there are two discrepancies we wish to comment on.

As already discussed with Fig. 5, the EW limit of Ouchi et al. (2008) at $z = 3.1$ (64 Å) has a dramatic effect on our model, since we predict very few objects with large EWs. As a consequence, if we reproduce the same EW cut, we again find less LAEs than these

authors (solid histogram in left-hand side panel of Fig. 8). To bypass this conflict, we may lower the EW cut we apply to our model until we find the same number density of LAEs. We obtain this match at ~ 50 Å, which is the value we had to apply to our modelled Lyα LF at $z = 3.1$ to fit the data from Ouchi et al. (2008). The UV LF of our model galaxies selected in this way is plotted as the dashed curve on Fig. 8. The good agreement we find now tells us that, provided we have the same number of objects, we manage to reproduce their UV luminosity distribution.

For other redshifts, the EW thresholds are lower, so that our lack of high EW is no longer a problem. However, our model does not match $z = 4.9$ data from Shioya et al. (2009), and we find many more UV-faint objects than they do. The reason of this disagreement is unclear, especially given that our model agrees with data from Ouchi et al. (2003) at the same redshift. This suggests that observations themselves may not agree one set with another and that more data is needed to shed light on this issue.

From this discussion, we conclude that our model is in broad agreement with observed UV properties of LAEs. And we once again demonstrate the special care that needs to be taken to reproduce selection effects.

We may now turn the question the other way around, and ask whether our model reproduces the Lyα properties of UV-selected galaxies. Shapley et al. (2003) studied the Lyα emission of LBGs at $z = 3$. They divided their LBG sample into four bins of Lyα EW and found that ∼25 per cent of LBGs have EWs > 20 Å and ∼50 per cent show Lyα emission (EW > 0 Å). It is not straightforward to apply the LBG selection to our model galaxies, and even more given the complex selections inherent to spectroscopic followups. Instead, here, we simply apply various rest-frame UV absolute magnitude cuts which should roughly bracket the selection of Shapley et al.

(2003). With a selection limit of $M_{1500} < -21$, we find that 28 per cent of the selected LBGs have EW > 20 Å and 69 per cent display Lyα emission (EW > 0 Å) at $z = 3.1$. Varying our selection limit, we find, for $M_{1500} < -21.5$ ($M_{1500} < -20.5$), that 25 per cent (39 per cent) of the objects have EW > 20 Å, and 74 per cent (71 per cent) of the selected LBGs are detected in emission. Thus the model predicts 1.75–3 times less LBGs with EW > 20 Å than LBGs simply displaying Lyα emission, whereas Shapley et al. (2003) found a factor of two. The discrepancy with their observations may come from the rest-frame selection instead of apparent magnitude selection, the value of the cut, and maybe the fact that they may have missed the detection of very faint Lyα lines (very low Lyα EW) in their sample.

5.3 Stellar masses of Lyα emitters

Fig. 9 plots the stellar mass distributions of LAEs divided into three Lyα luminosity bins at $z = 3.1$ and 4.9. Stellar mass distributions slowly shift to lower stellar masses by increasing the redshift. At intermediate redshifts, the results show the same behaviour as those at $z = 3.1$ and 4.9 so we do not show them here.
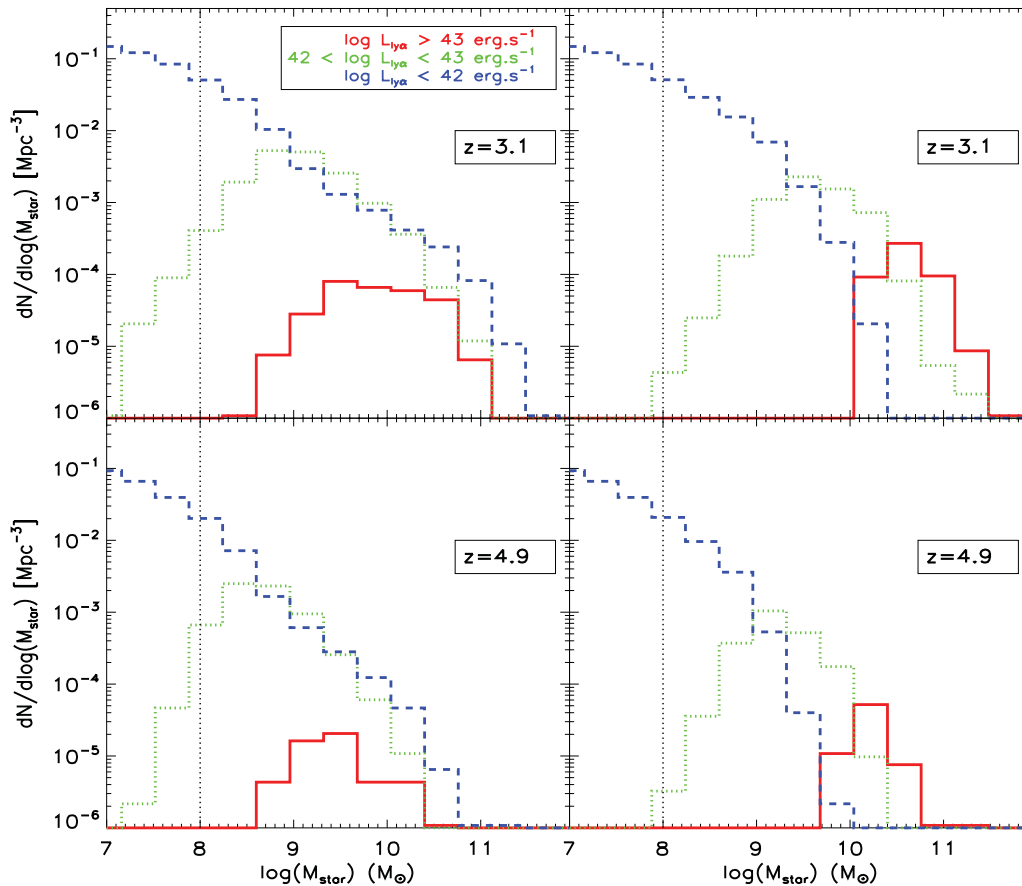

Figure 9. Distribution of the stellar masses divided in three bins of Lyα luminosity at $z = 3.1$ (top) and 4.9 (bottom). In each bin, the number of objects is divided by the bin size and the volume of the box. Solid red line: $L_{Lyα} > 10^{43}$ erg s^{-1}. Dotted green line: $10^{42} < L_{Lyα} < 10^{43}$ erg s^{-1}. In the left-hand column, we show the fiducial model results. Most massive galaxies are not the brightest LAEs as a consequence of their high dust extinction. The mass ranges spanned by bright LAEs ($L_{Lyα} > 10^{42}$ erg s^{-1}, corresponding to currently observed LAEs) broadly agree with observational estimates at various redshifts. In the right-hand column, we present the stellar mass distribution computed from the *constant Lyα escape fraction* model ($f_{esc} = 0.20$), for comparison with our fiducial model. In the *constant Lyα escape fraction* model, the stellar mass scales with the Lyα luminosity which predicts higher masses than what is observationally derived. The mass resolution effect of the simulation starts playing a role in the stellar mass distributions at ∼10^8 M$_\odot$ (vertical dotted line in each panel).

We compare the results of our fiducial model (left-hand column) and the $f_{esc} = 0.20$ model (right-hand column). As expected, in the latter model, brightest LAEs ($L_{Ly\alpha} > 10^{43}$ erg s^{-1}) have higher stellar masses, and fainter LAEs are less massive objects. It is expected since Lyα luminosities scale with SFRs which is tightly correlated to stellar mass at these redshifts. In our fiducial model, however, the behaviour is slightly different. If high Lyα luminosity objects have medium and rather large stellar masses (from 10^8 to 10^{11} M$_\odot$), the most massive objects ($>10^{11}$ M$_\odot$) are faint LAEs ($L_{Ly\alpha} < 10^{41}$ erg s^{-1}). This is a consequence of the nearly flat Lyα escape fraction distribution that we find for high SFR (massive) objects (Fig. 3). For the largest fraction of LAEs which are currently observed ($L_{Ly\alpha} > 10^{42}$ erg s^{-1}), we predict stellar masses ranging from 10^7 to 10^{11} M$_\odot$.

At $z = 3.1$, Gawiser et al. (2006) find a mean stellar mass of 5×10^8 M$_\odot$ which agrees with the mean value predicted by our fiducial model for LAEs in the range $10^{42} < L_{Ly\alpha} < 10^{43}$ erg s^{-1}. The *constant Lyα escape fraction* model predicts, however, a mean value almost ten times higher for this luminosity range.

Massive LAEs (10^{10-11} M$_\odot$) recently observed at $z = 3-4$ by Ono et al. (2010) have Lyα luminosties comprised between $\sim 10^{42}$ and 2×10^{43} erg s^{-1}. Those more massive galaxies fit in the range of prediction of our model (green and red curves of the top left-hand panel of Fig. 9).

LAEs reported by Finkelstein et al. (2007) at $z = 4.5$ have stellar masses ranging from 2×10^7 to 2×10^9 M$_\odot$. For $L_{Ly\alpha} > 10^{42}$ erg s^{-1}, the fiducial model yields a mass range from 2×10^7 to 2×10^{10} M$_\odot$, whereas the *constant Lyα escape fraction* model predicts higher masses.

Pirzkal et al. (2007) observed LAEs with $L_{Ly\alpha} > 2 \times 10^{42}$ erg s^{-1} having $10^7 < M_{star} < 2 \times 10^9$ M$_\odot$ at $z \sim 5$, which is rather similar to the results obtained from the fiducial model at $z = 4.9$, and below the interval spanned by the *constant Lyα escape fraction* model.

Therefore, in the redshift range $3 < z < 5$, our model gives stellar masses for bright LAEs ($L_{Ly\alpha} > 10^{42}$ erg s^{-1}) closer to what is observed than the *constant Lyα escape fraction* model, and naturally recovers the observational fact that LAEs which are currently observed are not very massive objects.

5.4 Ando effect

Many authors reported a deficit of high Lyα EW (>100 Å) in UV bright objects ($M_{1500} < -22$) between $z = 3$ and 6 (Ando et al. 2006; Shimasaku et al. 2006; Ouchi et al. 2008; Stark et al. 2010). We will refer to this effect as the Ando effect. It has also been discussed in theoretical papers (Verhamme et al. 2008; Kobayashi et al. 2010). The reasons invoked to explain this effect are multiple: the time sequence of a starburst, resonant scattering in the gas, a clumpy dust distribution and/or the age of the stellar population. We investigate this feature with our model and plot our results in Fig. 10. We find that we recover this effect at $3 < z < 5$. Since our model does not reproduce very accurately the observed Lyα EW, we do not compare with observational data, but we only discuss the effect qualitatively.

To see why our model predicts this lack of high Lyα EW in UV bright galaxies, we show the relation between the dust-uncorrected UV magnitude, and the intrinsic Lyα EW in Fig. 11. There is almost no correlation between those two quantities, except that the highest intrinsic Lyα EWs come from UV faint galaxies. It is due to the fact that UV bright objects have old stellar populations, whereas fainter galaxies display a whole range of ages. A fraction of the UV-faint objects are young, so that they have a high ratio of ionizing lumi-
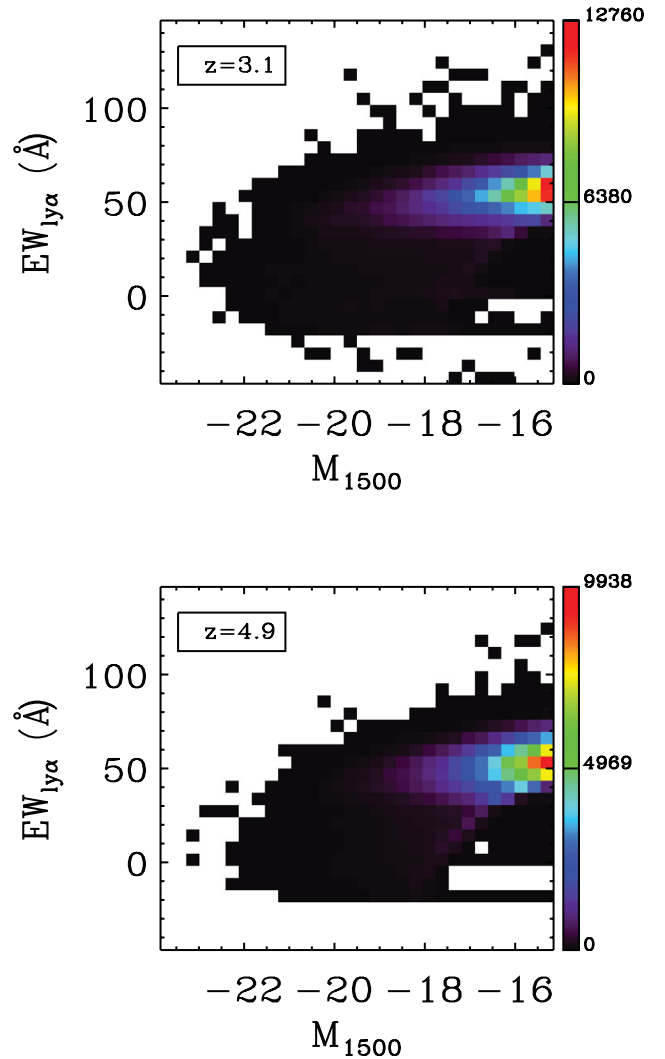

Figure 10. Observed Lyα EW versus the UV magnitude at 1500 Å for the fiducial model at $z = 3.1$ and 4.9. The colour of each pixel represent the number of objects in that pixel.

nosity over UV-continuum luminosity $L_{\lambda < 912}/L_{cont}$ which produces large intrinsic Lyα EWs. This ratio is, on average, smaller for older, UV-brighter galaxies, so that large intrinsic Lyα EWs do not exist for those objects. From this study of the galaxy SEDs, we are able to find part of the explanation of the absence of high Lyα EWs among UV-bright objects.

Looking again at Fig. 10, we can see that this lack is more significant for the observed Lyα EW (after radiative transfer) than in the M_{1500}^{uncorr}–EW$_{Ly\alpha}^{intr}$ plane (Fig. 11). In our model, H I column densities (and dust opacities, by construction of the dust opacity in our model) take large values for UV-bright galaxies, as shown by Fig. 12. We then argue that, in those galaxies, Lyα photons are more extinguished than in UV-faint galaxies, because of the resonance of the Lyα line in a dense, dusty medium.

As we do not reproduce the observed distribution of Lyα EWs at high values (>150 Å), we have to be prudent with our conclusions. We can wonder what would be the impact of the physical effects that we identified as a possible explanation for very large Lyα EWs on the Ando effect. Would clumpiness and resolved starbursts (young stellar populations) lead to high Lyα EW values in UV bright or faint galaxies preferentially? A possible answer can be
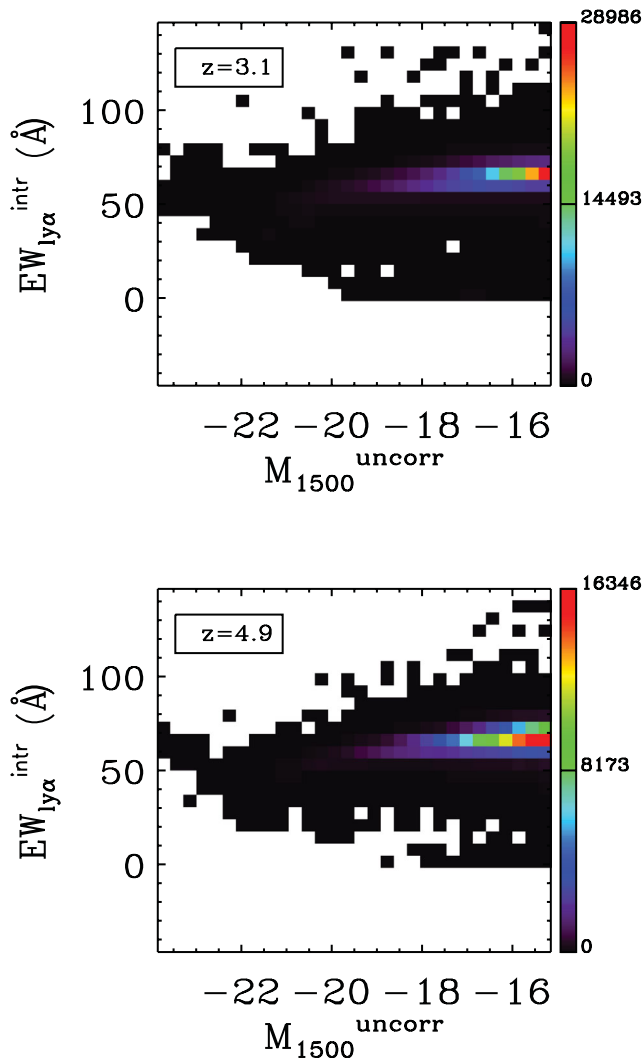
Figure 11. Intrinsic Lyα EW versus the dust-uncorrected UV magnitude at 1500 Å for the fiducial model at $z = 3.1$ and 4.9. The colour of each pixel represent the number of objects in that pixel.

inferred from Kobayashi et al. (2010). They find that these two effects lead to smaller (larger) Lyα EWs in UV brighter (fainter) galaxies. Then, the no-reproduction of large Lyα EWs in our model should not impact our interpretation of the Ando effect.

Therefore, we find two main reasons to explain the Ando effect in our model: (i) UV-bright galaxies are old, so that they do not show high intrinsic Lyα EWs and (ii) H I column densities for UV-bright objects are larger, which leads to an enhanced destruction of Lyα photons as a consequence of radiation transfer effects, as already suggested by Verhamme et al. (2008).

6 DISCUSSION AND CONCLUSIONS

In this paper, we have presented a new semi-analytic model for high redshift LAEs. We have investigated the Lyα emission and transfer processes taking into account resonant scattering effects through gas outflows. To this aim, we have coupled the output of the GALICS semi-analytic model with results of Monte Carlo radiation transfer runs which compute the Lyα transfer through static and expanding shells. We had to make a few simplifying assumptions (central emission, sphericity and homogeneity of the
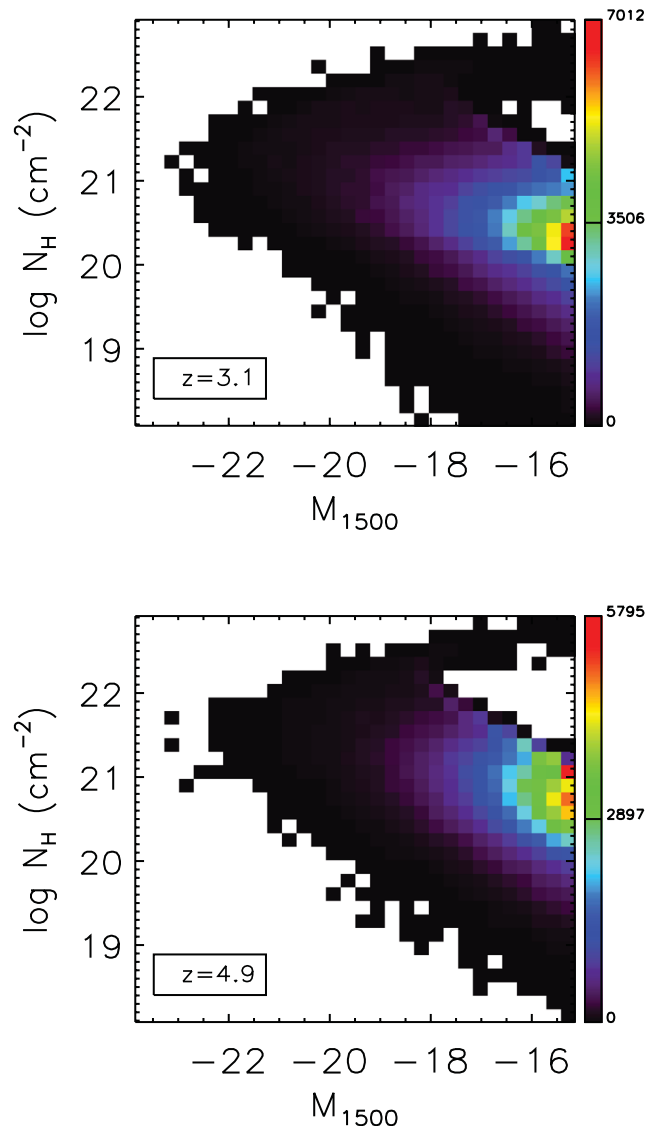

Figure 12. H I shell column density versus the UV magnitude at 1500 Å for the fiducial model at $z = 3.1$ and 4.9. The colour of each pixel represent the number of objects in that pixel. The no-data area (white hole) at $M_{1500} \sim 16$ and $\log(N_H) \sim 22$ is due to the fact that (i) $\log(N_H)$ is correlated to the dust-uncorrected magnitude $M_{1500}^{\mathrm{uncorr}}$ (both proportional to the galaxy mass), and (ii) τ_{dust} is proportional to (N_H) (equation 2). This implies that intrinsically bright UV galaxies, in our model, have large $\log(N_H)$ values and are strongly extinguished, in terms of UV magnitude, by $\sim -2.5 \times \log[\exp(-\tau_{\mathrm{dust}})] \sim \tau_{\mathrm{dust}} \propto N_H$. This makes the rightward shift of large $\log(N_H)$ points in this figure.

shell), and to use relations for the expanding shell that scale with the physical properties of the galaxies as they are computed by the semi-analytic model.

We have run this new model on a high-resolution N-body simulation (1024^3 particles) of a large cosmological volume [$V = (100\,h^{-1})^3$ Mpc^3] of DM. Then, we have enough statistics for massive, rare objects, and enough resolution for less massive objects ($M_{\mathrm{halo}}^{\mathrm{min}} = 1.70 \times 10^9$ M$_\odot$). In this first paper, we aim at getting a coherent view of LAEs. We fit the UV LF at $z = 3$–5 on a compilation of available data (Fig. 1) by adopting a high normalization of the SFR, that, in any case, scales with gas mass as in Kennicutt's local relation. Then, we get the following results.

(i) The Lyα escape fraction for each galaxy is obtained by taking into account the resonant nature of the Lyα line. This is in sharp contrast with the assumptions made in previous semi-analytical models. The distribution of f_{esc} is broad, and we see a trend with stellar masses of galaxies (Fig. 3). Low-mass galaxies have f_{esc} of the order of unity, and massive galaxies span a broad range of f_{esc} values.

(ii) Because of this trend, the resulting Lyα LFs are steeper from bright to faint luminosities than observed in simpler toy models (*constant Lyα escape fraction*, *screen* and *slab*).

(iii) Lyα LFs are well reproduced between $z = 3$ and 5 (Fig. 4) without any additional free parameter in the Lyα model. More specifically, low-luminosity data from Rauch et al. (2008) at $z \sim 3$ are reproduced, so that we predict more faint LAEs than commonly used *constant Lyα escape fraction* models.

(iv) We have shown that Lyα LFs are sensitive to Lyα EW cuts (Fig. 5). This may explain the scatter in the compilation of data, since surveys (both spectroscopic and narrow-band) are subject to different Lyα EW selection limits.

(v) The IGM attenuation of Lyα photons is very weak in our model, because the predicted Lyα spectra are redshifted with respect to the Lyα line centre, as a consequence of the scatter of Lyα photons in the expanding shell (Fig. 6). Therefore, in our model, the Lyα transfer within the shell alone explains the observed luminosities of LAEs.

(vi) The predicted distributions of Lyα EWs are narrower than the data (Fig. 7). About 85 per cent of the observed samples have $0 < EW < 150$ Å, and can roughly be reproduced by the model. However, we predict very few objects with EW > 150 Å, whereas some are observed. Effects that are not included in the model, such as short bursts of star formation, a top-heavy IMF, population III stars and/or dust clumpiness, may be the cause of such high Lyα EWs. On the other hand, even without invoking such processes, our fiducial model is able to recover roughly the bulk of the EW distribution.

(vii) The UV LFs of LAEs are in agreement with most data, with some discrepancies (Fig. 8). The scatter in the data may be due to poorly controlled selection criteria.

(viii) We find that our predictions of the fraction of Lyα emitting LBGs follow the same trend as the one found by Shapley et al. (2003), that is to say, approximately two times less LBGs having EW > 20 Å than LBGs having EW > 0 Å. However, our LBG selection (in rest-frame magnitude) is somehow arbitrary since, in this study, we do not attempt to take into account the apparent colours and magnitudes that are necessary to select LBGs correctly.

(ix) Whereas in a simple *constant Lyα escape fraction* model, Lyα luminosities scale with stellar masses, we find that most massive objects are faint LAEs (Fig. 9). Our predicted stellar masses for rather bright LAEs are in correct agreement with observational estimates which find that LAEs are intermediate-mass objects.

(x) The deficit of high Lyα EWs (the Ando effect) that is found in UV-bright galaxies is well reproduced by our model (Fig. 10). The absence of such large Lyα EWs comes from the fact that H I column densities are high for UV-bright objects, which preferentially extinguishes Lyα photons, as already suggested by Verhamme et al. (2008). Moreover, UV-bright (and consequently massive) galaxies host older stellar populations which prevent them from having high intrinsic Lyα EWs.

Despite some discrepancies with specific data sets, the overall picture seems to be quite satisfactory, given the crudeness of the assumptions. Most of the observational constraints on high redshift LAEs are well recovered by our model.

Although the coupling of the semi-analytic model with Lyα radiation transfer is admittedly very crude, our global description seems to catch the intuitive trend according to which fainter galaxies, on an average, are more transparent for Lyα photons.

The hypothesis that gas outflows (with speed from a few tens to hundreds km s^{-1}) are common in high redshift galaxies is well supported by observations. With such a model, we have been able to agree with many observational data and we found no need to invoke the influence of gas infalls on the Lyα line. Indeed, it has already been shown that it is hard to recover the redward asymetry of the Lyα line with models of Lyα radiative transfer through infalling neutral gas (Verhamme et al. 2006; Dijkstra, Lidz & Wyithe 2007).

Obviously more refined models are still necessary, to relax some of the assumptions, especially spherical symmetry and homogeneity of the shell. The cases for more realistic geometries and the effect of galaxy inclination are being investigated (Verhamme et al. 2012).

The simulation we used in this paper has been run with initial conditions in agreement with the *WMAP*3 release, in which the σ_8 value is low. Structure growth is delayed with this low normalization of the power spectrum, and fewer objects form at high redshift. This choice has consequences on our ability to reproduce galaxies beyond $z = 6$, and we somehow correct this effect for lower redshifts (3–5) by normalizing the SFR parameter in order to fit the UV LFs. New simulations with an up-to-date cosmology (*WMAP*5/7), where the derived σ_8 value is larger, can help to investigate higher redshifts with our approach.

Even if the number of detections of LAEs is always increasing, the data are still quite heterogeneous. Forthcoming LAE surveys with the Hobby-Eberly Telescope Dark Energy Experiment (HETDEX, Hill et al. 2008) (z < 3.8; bright objects only), and the *Multi Unit Spectroscopic Explorer* (*MUSE*, Bacon et al. 2006) at the Very Large Telescope (2.8 < z < 6.7) should produce more coherent data sets. In a forthcoming paper (Garel et al., in preparation), we will present predictions for *MUSE* observations with our model.

REFERENCES

Ando M., Ohta K., Iwata I., Akiyama M., Aoki K., Tamura N., 2006, ApJ, 645, L9
Arnouts S. et al., 2005, ApJ, 619, L43
Bacon R. et al., 2006, The Messenger, 124, 5
Baker A. J., Tacconi L. J., Genzel R., Lehnert M. D., Lutz D., 2004, ApJ, 604, 125
Bertone S., Stoehr F., White S. D. M., 2005, MNRAS, 359, 1201

Blaizot J., Guiderdoni B., Devriendt J. E. G., Bouchet F. R., Hatton S. J., Stoehr F., 2004, MNRAS, 352, 571

Blanc G. A. et al. 2011, ApJ, 736, 31

Bouwens R. J., Illingworth G. D., Franx M., Ford H., 2007, ApJ, 670, 928

Cattaneo A., Dekel A., Faber S. M., Guiderdoni B., 2008, MNRAS, 389, 567

Charlot S., Fall S. M., 1993, ApJ, 415, 580

Dawson S., Spinrad H., Stern D., Dey A., van Breugel W., de Vries W., Reuland M., 2002, ApJ, 570, 92

Dawson S., Rhoads J. E., Malhotra S., Stern D., Wang J., Dey A., Spinrad H., Jannuzi B. T., 2007, ApJ, 671, 1227

Dayal P., Ferrara A., Gallerani S., 2008, MNRAS, 389, 1683

Dekel A., Birnboim Y., 2006, MNRAS, 368, 2

Devriendt J. E. G., Guiderdoni B., Sadat R., 1999, A&A, 350, 381

Dijkstra M., Loeb A., 2008, MNRAS, 391, 457

Dijkstra M., Wyithe J. S. B., 2010, MNRAS, 408, 352

Dijkstra M., Haiman Z., Spaans M., 2006, ApJ, 649, 14

Dijkstra M., Lidz A., Wyithe J. S. B., 2007, MNRAS, 377, 1175

Finkelstein S. L., Rhoads J. E., Malhotra S., Pirzkal N., Wang J., 2007, ApJ, 660, 1023

Furlanetto S. R., Schaye J., Springel V., Hernquist L., 2005, ApJ, 622, 7

Gabasch A. et al., 2004, A&A, 421, 41

Gawiser E. et al., 2006, ApJ, 642, L13

Gronwall C. et al., 2007, ApJ, 667, 79

Haiman Z., 2002, ApJ, 576, L1

Hansen M., Oh S. P., 2006, MNRAS, 367, 979

Hatton S., Devriendt J. E. G., Ninin S., Bouchet F. R., Guiderdoni B., Vibert D., 2003, MNRAS, 343, 75

Hayes M. et al., 2010, Nat, 464, 562

Hill G. J. et al., 2008, in Kodama T., Yamada T., Aoki K., eds, ASP Conf. Ser. Vol. 399, The Hobby-Eberly Telescope Dark Energy Experiment (HETDEX): Description and Early Pilot Survey Results. Astron. Soc. Pac., San Francisco, p. 115

Hu E. M., Cowie L. L., McMahon R. G., 1998, ApJ, 502, L99

Hu E. M., Cowie L. L., Barger A. J., Capak P., Kakazu Y., Trouille L., 2010, ApJ, 725, 394

Iwata I., Ohta K., Tamura N., Akiyama M., Aoki K., Ando M., Kiuchi G., Sawicki M., 2007, MNRAS, 376, 1557

Kennicutt R. C., Jr, 1983, ApJ, 272, 54

Kennicutt R. C., Jr, 1998, ApJ, 498, 541

Kitzbichler M. G., White S. D. M., 2007, MNRAS, 376, 2

Kobayashi M. A. R., Totani T., Nagashima M., 2007, ApJ, 670, 919

Kobayashi M. A. R., Totani T., Nagashima M., 2010, ApJ, 708, 1119

Kudritzki R. et al., 2000, ApJ, 536, 19

Kunth D., Mas-Hesse J. M., Terlevich E., Terlevich R., Lequeux J., Fall S. M., 1998, A&A, 334, 11

Laursen P., Sommer-Larsen J., 2007, ApJ, 657, L69

Laursen P., Sommer-Larsen J., Andersen A. C., 2009, ApJ, 704, 1640

Le Delliou M., Lacey C., Baugh C. M., Guiderdoni B., Bacon R., Courtois H., Sousbie T., Morris S. L., 2005, MNRAS, 357, L11

Le Delliou M., Lacey C. G., Baugh C. M., Morris S. L., 2006, MNRAS, 365, 712

Madau P., 1995, ApJ, 441, 18

Mao J., Lapi A., Granato G. L., de Zotti G., Danese L., 2007, ApJ, 667, 655

Mas-Hesse J. M., Kunth D., Tenorio-Tagle G., Leitherer C., Terlevich R. J., Terlevich E., 2003, ApJ, 598, 858

Mathis J. S., Mezger P. G., Panagia N., 1983, A&A, 128, 212

McLinden E., Finkelstein S. L., Rhoads J. E., Malhotra S., Hibon P., Richardson M., 2011, BAAS, 43, 33543

McLure R. J., Cirasuolo M., Dunlop J. S., Foucaud S., Almaini O., 2009, MNRAS, 395, 2196

Nagamine K., Ouchi M., Springel V., Hernquist L., 2010, PASJ, 62, 1455

Neufeld D. A., 1991, ApJ, 370, L85

Okamoto T., Gao L., Theuns T., 2008, MNRAS, 390, 920

Ono Y. et al., 2010, MNRAS, 402, 1580

Osterbrock D. E., 1989, Astrophysics of Gaseous Nebulae and Active Galactic Nuclei. University Science Books, Mill Valley, CA

Ouchi M. et al., 2003, ApJ, 582, 60

Ouchi M. et al., 2008, ApJS, 176, 301

Ouchi M. et al., 2010, ApJ, 723, 869

Partridge R. B., Peebles P. J. E., 1967, ApJ, 147, 868

Pettini M., Kellogg M., Steidel C. C., Dickinson M., Adelberger K. L., Giavalisco M., 1998, ApJ, 508, 539

Pettini M., Shapley A. E., Steidel C. C., Cuby J., Dickinson M., Moorwood A. F. M., Adelberger K. L., Giavalisco M., 2001, ApJ, 554, 981

Pirzkal N., Malhotra S., Rhoads J. E., Xu C., 2007, ApJ, 667, 49

Rauch M. et al., 2008, ApJ, 681, 856

Reddy N. A., Steidel C. C., Fadda D., Yan L., Pettini M., Shapley A. E., Erb D. K., Adelberger K. L., 2006, ApJ, 644, 792

Reddy N. A., Steidel C. C., Pettini M., Adelberger K. L., Shapley A. E., Erb D. K., Dickinson M., 2008, ApJS, 175, 48

Samui S., Srianand R., Subramanian K., 2009, MNRAS, 398, 2061

Santos M. R., Ellis R. S., Kneib J., Richard J., Kuijken K., 2004, ApJ, 606, 683

Sawicki M., Thompson D., 2006, ApJ, 648, 299

Schaerer D., Hayes M., Verhamme A., Teyssier R., 2011, A&A, 531, A12

Shapley A. E., Steidel C. C., Pettini M., Adelberger K. L., 2003, ApJ, 588, 65

Shimasaku K. et al., 2006, PASJ, 58, 313

Shioya Y. et al., 2009, ApJ, 696, 546

Shu C., Mo H., Shu-DeMao, 2005, Chinese J. Astron. Astrophys., 5, 327

Somerville R. S., Primack J. R., Faber S. M., 2001, MNRAS, 320, 504

Spergel D. N. et al., 2007, ApJS, 170, 377

Springel V., 2005, MNRAS, 364, 1105

Stark D. P., Ellis R. S., Chiu K., Ouchi M., Bunker A., 2010, MNRAS, 408, 1628

Steidel C. C., Adelberger K. L., Giavalisco M., Dickinson M., Pettini M., 1999, ApJ, 519, 1

Tapken C., Appenzeller I., Mehlert D., Noll S., Richling S., 2004, A&A, 416, L1

Tapken C. et al., 2006, A&A, 455, 145

Tapken C., Appenzeller I., Noll S., Richling S., Heidt J., Meinköhn E., Mehlert D., 2007, A&A, 467, 63

Tenorio-Tagle G., Silich S. A., Kunth D., Terlevich E., Terlevich R., 1999, MNRAS, 309, 332

Tilvi V., Malhotra S., Rhoads J. E., Scannapieco E., Thacker R. J., Iliev I. T., Mellema G., 2009, ApJ, 704, 724

Tweed D., Devriendt J., Blaizot J., Colombi S., Slyz A., 2009, A&A, 506, 647

Valls-Gabaud D., 1993, ApJ, 419, 7

van Breukelen C., Jarvis M. J., Venemans B. P., 2005, MNRAS, 359, 895

Verhamme A., Schaerer D., Maselli A., 2006, A&A, 460, 397

Verhamme A., Schaerer D., Atek H., Tapken C., 2008, A&A, 491, 89

Verhamme A., Dubois Y., Blaizot J., Garel T., Bacon R., Devriendt J., Guiderdoni B., Slyz A., 2012, A&A, submitted

Wang J., Malhotra S., Rhoads J. E., Zhang H., Finkelstein S. L., 2009, ApJ, 706, 762

Zheng Z., Miralda Escudé J., 2002, ApJ, 578, 33

Zheng Z., Cen R., Trac H., Miralda Escudé J., 2010, ApJ, 716, 574

This paper has been typeset from a TEX/LATEX file prepared by the author.